Bulletin of Mathematical Biology (2007) 69: 289–327
DOI 10.1007/s11538-005-9036-x

ORIGINAL ARTICLE

A Viscoelastic Traction Layer Model of Muco-Ciliary Transport

D. J. Smith*, E. A. Gaffney, J. R. Blake

School of Mathematics, University of Birmingham, Birmingham B15 2TT, UK

Received: 1 March 2006 / Accepted: 22 March 2006 / Published online: 28 June 2006

Abstract A new mathematical model of the transport of mucus and periciliary liquid (PCL) in the airways by cilia is presented. Mucus is represented by a linearly viscoelastic fluid, the mat of cilia is modelled as an 'active porous medium.' The propulsive effect of the cilia is modelled by a time-dependent force acting in a shear-thinned 'traction layer' between the mucus and the PCL. The effects of surface and interface tension are modelled by constraining the mucus free surface and mucus–PCL interface to be flat. It is assumed that the epithelium is impermeable to fluid. Using Fourier series, the system is converted into ODEs and solved numerically. We calculate values for mean mucus speed close to those observed by Matsui et al. [J. Clin. Invest., 102(6):1125–1131, 1998], ($\sim 40\ \mu\mathrm{m\,s^{-1}}$). We obtain more detail regarding the dynamics of the flow and the nonlinear relationships between physical parameters in healthy and diseased states than in previously published models. Pressure gradients in the PCL caused by interface and surface tension are vital to ensuring efficient transport of mucus, and the role of the mucus–PCL interface appears to be to support such pressure gradients, ensuring efficient transport. Mean transport of PCL is found to be very small, consistent with previous analyses, providing insight into theories regarding the normal tonicity of PCL.

Keywords Mucus · Cilia · Muco-ciliary clearance · Salt–fluid controversy · Periciliary liquid transport

1. Introduction

In this paper we describe a 'traction layer' model of muco-ciliary transport. The model considers the airway surface liquid (ASL) as three fluid layers, the lower layer being Newtonian, the remaining two being linearly viscoelastic. The propulsive force produced by the cilia is modelled by a volume force which acts in the

*Corresponding author.
E-mail addresses: smithd@for.mat.bham.ac.uk (D. J. Smith), eag@for.mat.bham.ac.uk (E. A. Gaffney), J.R.Blake@bham.ac.uk (J. R. Blake).

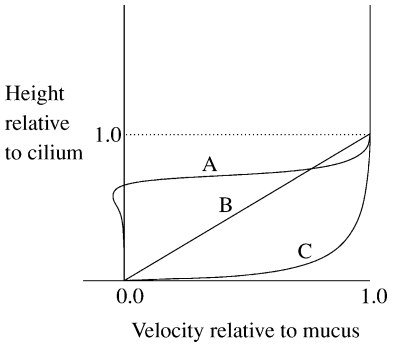

Fig. 1 Comparing the velocity profiles predicted by theory (typified by A), shear-driven flow (B) and those apparently found by experiment (C). Redrawn from Matsui et al. (1998).

region—the traction layer—where the cilia penetrate the mucus, varying spatially and temporally with the metachronal wave. The effect of the beating cilia on the flow in the PCL is modelled using the 'active porous medium' ideas first presented in Blake (1975a). A possible shear-thinning effect in the traction layer is included. By using Fourier series analysis we exploit periodicity and convert the system of PDEs to a system of ODEs which are solved numerically.

This study is motivated by the salt–fluid controversy described by Guggino (2001) regarding the normal tonicity of ASL and hence the pathogenesis of cystic fibrosis. Briefly, the hypotonic defensin hypothesis (Smith et al., 1996) states that the epithelium is impermeable to fluid. This is consistent with very low mean transport of PCL along the converging airways of the lung. Low mean PCL transport was predicted by the physical models of Fulford and Blake (1986) and Blake and Winet (1980), as depicted in Fig. 1A. The isotonic volume hypothesis (Boucher, 1994) states that there are large fluxes of fluid across the epithelium. This is consistent with significant mean transport of PCL along the airways. Human tracheobronchial epithelial culture tracer dispersion experiments conducted by Matsui et al. (1998) appear to show approximately equal and significant transport of PCL and mucus, as depicted in Fig. 1C. In this study we model the hypotonic defensin hypothesis by considering the fluid flow in the PCL and mucus, determining the mean transport of PCL and time-dependent fluctuations subject to the no-slip, no-flux condition on the epithelium. The detailed information we obtain regarding the spatial and temporal variations in the muco-ciliary flow will be useful for conducting tracer dispersion simulations such as those described in Blake and Gaffney (2001) and Smith et al. (2006). In addition, we obtain a detailed understanding of the nonlinear response of the system to altered physical parameters, and the importance of surface and interface tension.

2. Review of muco-ciliary modelling

The earliest attempt to model muco-ciliary flow mathematically was that of Barton and Raynor (1967), modelling the cilium as a rigid rod which automatically shortens during the recovery stroke. This approach has several serious limitations, in

particular, the motion of the cilia is not accurately modelled and the metachronal wave is not included (Blake, 1973). However, their work was a forerunner of later 'cilia sublayer' models, and they calculated realistic flow rates. Their characterisation of the cilium as a rigid rod is exploited in Section 4.

The model of Ross (1971) took into account the non-Newtonian nature of the upper mucous layer. The mucus–cilia interface was modelled as an impermeable 'wavy wall,' mucus was modelled as a nonlinear Maxwell fluid, and the resulting system of equations was solved analytically using Fourier series and asymptotic expansions in the amplitude of the metachronal wave. Mucus flow rates were calculated which were in rough agreement with experimental data, but flow in the PCL was not modelled. It has been noted (Blake, 1972) that at velocities found in nature, wavy wall models are not adequate for systems, such as that found in the lung, exhibiting antiplectic metachronism since the tips of the cilia may be widely spaced during the effective stroke. Hence, representing the tips of the cilia with a no-slip boundary is not appropriate. Nor did the model of Ross (1971) adequately represent the effect of the cilia recovery stroke taking place below the mucus–PCL interface.

An alternative 'cilia sublayer' approach was developed by Blake (1972), initially for ciliated micro-organisms. Due to their slenderness, the cilia could be modelled by distributing force singularities along their centre-lines. These ideas were extended in later papers including Liron and Mochon (1976) and Fulford and Blake (1986). A detailed review of such models is given in Smith (2006).

For a genuinely accurate model, the ASL needs to be considered as at least two separate layers, the lower being watery and nearly Newtonian, the upper being viscous and non-Newtonian. Blake (1975b) applied the discrete sublayer model to such a system, comparing the relative importance of muco-ciliary transport, gravity and clearance due to air flow. The model differed from most in this field in that the cilia were assumed to be synchronised rather than forming a metachronal wave, based on the fact that the cilia in the lung are very closely packed, at least on an individual cell. Limitations of this work were that there was no penetration into the mucous layer by cilia, and the cilia beat cycle used was not particularly accurate. These limitations were addressed in Fulford and Blake (1986), where the cilia beat cycles found by Sleigh (1977) and Sanderson and Sleigh (1981) were used, together with resistance coefficients for a slender body 'straddling' the interface between two fluids of differing viscosity. They were also able to examine the effects of having a large number of inactive cilia, as in a diseased lung. However, the upper layer was modelled as a Newtonian fluid, and only a time-averaged profile was obtained.

Keller (1975) developed a different approach to modelling the sublayer, known as the 'continuum sublayer' or 'traction layer' model. The action of the cilia is modelled as a spatially continuous volume force. This technique was applied to ciliated micro-organisms where the mucous layer need not be considered. Exploiting the periodicity of the ciliary beat, Fourier analysis was used to find the stream function for Stokes flow in terms of the force distribution. The force distribution was found using the resistive force theory of Gray and Hancock together with expressions for the resistance coefficients derived by Chwang and Wu (1975) for a slender ellipsoid. Blake and Winet (1980) applied the traction layer approach to mucociliary

transport in the lung, using the idealised beat pattern of Barton and Raynor (1967). They considered both the PCL and the mucous layers, but modelled mucus as a Newtonian fluid, calculating time-averaged flow only. They also attempted to take into account the resistance of the cilia sublayer by modelling it as an 'active porous medium,' building on the earlier paper of Blake (1977). Their results suggested that slight penetration into the mucous layer by the cilia substantially enhanced transport. They predicted that mean PCL transport would be very small.

Liron and Rozenson (1983) examined tip penetration in a different way. They modelled mucus as a non-Newtonian fluid with the linearised Oldroyd equations, valid for small rates of shear. They assumed that the only forces driving the fluids were a constant pressure gradient and a series of impulses, represented by Dirac delta functions, produced by the cilium tips. After solving the resulting equations by Fourier transforms they concluded that penetration was necessary for transport. However, their approach did not take into account the resistance of the cilia sublayer (Fulford and Blake, 1986).

In a more recent paper, King et al. (1993) formulated a simple analytical model of the muco-ciliary system designed to test the effect of mucus viscoelasticity. They predicted, amongst other things, that mucus transport increases as the shear modulus of elasticity decreases. However, their model is limited in a number of ways—they assumed that there was no net transport of PCL in the cilia sublayer, a property our model is designed to test, they only took into account steady motion of the PCL, whereas oscillatory motion may prove important for mixing effects (Matsui et al., 1998), and assumed that there was a layer of PCL between the top of the cilia sublayer and the mucous layer, whereas micrographs taken by Puchelle et al. (1998) appear to show the cilia penetrating the mucus.

3. The traction layer model

Motivated by the need to understand the salt–fluid controversy, Barlow (2000) developed a simple Newtonian traction layer model of muco-ciliary transport which formed a starting point for the more detailed model described in this work. We treat the ASL as three fluid layers separated by flat interfaces at $y = h$ and $y = L$, as shown in Fig. 2. This assumption seems reasonable if we examine the micrographs of Sanderson and Sleigh (1981), in which the mucus–PCL interface is shown to be remarkably flat, even when there are large undulations in the epithelium—which are not present in the experiments of Matsui et al. (1998). The parameter h is the depth of the PCL, L is the length of the cilia, H is the depth of the ASL. In this paper we consider a two-dimensional model of the ASL, as shown in Fig. 2. We refer to the direction of transport, the x_1 direction, as the x or the 'horizontal' direction. We refer to the direction normal to the epithelium, the x_3 direction, as the y or the 'vertical' direction.

The lower layer $0 < y < h$, representing the PCL, is modelled by a Newtonian fluid of viscosity μ^{P}. We take $\mu^{\mathrm{P}} = 0.001\,\mathrm{N\,m^{-2}\,s}$, as for water. The traction layer region $h < y < L$, representing the region in which the cilia penetrate the mucus, is modelled by a Maxwell viscoelastic fluid with viscosity μ^{M1} and relaxation time λ_1. The upper layer $L < y < H$, representing the mucus above the penetration region,

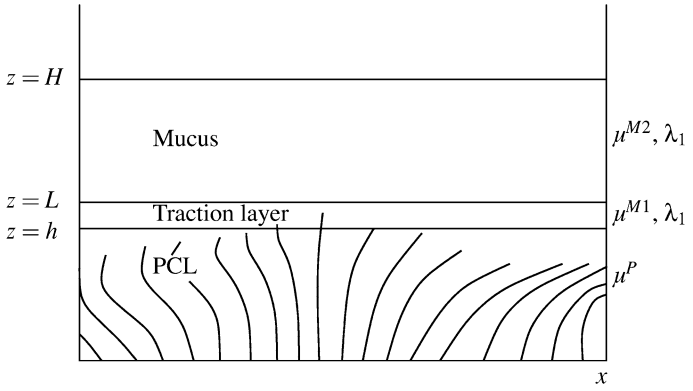

Fig. 2 Diagram of the three-layer model. Newtonian PCL, viscosity μ^{P}, depth h. Traction layer, viscosity μ^{M1}, elasticity λ_1, depth $L-h$. Mucus layer, viscosity μ^{M2}, elasticity λ_1, depth $H-L$.

is modelled by a Maxwell fluid of viscosity μ^{M2} and the same relaxation time λ_1. In general, $\mu^{\mathrm{M1}} < \mu^{\mathrm{M2}}$ because mucus is shear thinning and the shear forces in the traction layer will be larger than above the traction layer. We shall discuss the values of these parameters in Section 5.

The parameter h will be approximately 5 μm, L will be about 5–6 μm, and $H-L$, depending on the thickness of the upper mucous layer, may vary from just 0 to 2 μm, corresponding to the terminal bronchii, up to an average of 15 μm, or more in pathological conditions or in the trachea. The mucous layer is still thicker in the pharynx and nasal passage, but we shall not be concerned with these regions (data from ICRP, 1994).

Through momentum balance, one can derive the following form of the Navier–Stokes momentum equations:

$$\sigma_{jk,k} + f_j = \rho \frac{Du_j}{Dt}, \tag{1}$$

where σ_{jk} is the stress tensor, f_j the body force (force per unit volume) on the fluid representing the action of the cilia, ρ the density and u_j the fluid velocity, with summation over repeated indices and the comma denoting differentiation with respect to the following index. D/Dt represents the convective derivative $\partial/\partial t + u_i \partial/\partial x_i$.

From the parameters given in ICRP (1994), we take scalings $U = 40 \times 10^{-6}\,\mathrm{m\,s^{-1}}$ for velocity, $L = 6 \times 10^{-6}\,\mathrm{m}$ for length, $\rho = 1000\,\mathrm{kg\,m^{-3}}$ for density and $\mu = \mu^{\mathrm{P}} = 0.001\,\mathrm{Nm^{-2}s}$ for viscosity. The Reynolds number $\rho UL/\mu$ is approximately 2×10^{-4}, so we neglect the convective term. In addition, the nondimensional parameter $\sigma\rho L^2/\mu$ will be of the order of 2×10^{-3} since the frequency σ will be of the order of $60\,\mathrm{rad\,s^{-1}}$, so we neglect the time-dependent term $\partial u_j/\partial t$ and obtain

$$\sigma_{jk,k} + f_j = 0, \tag{2}$$

in dimensional variables. In addition to this, we require the equation of mass conservation. For an incompressible fluid this is

$$u_{j,j} = 0. \tag{3}$$

Given appropriate boundary conditions and expressions for the force, we shall solve Eqs. (2) and (3) in the three fluid layers.

4. Modelling the volume force exerted by the cilia

As discussed above, we write the force on the fluid as the sum of a propulsive force in the traction layer and a resistive force in the PCL, $\mathbf{f} = \mathbf{f}_{\text{prop}} + \mathbf{f}_{\text{res}}$. Gravity is neglected in this model, since except for diseased lungs with greatly thickened mucous its effect is negligible (Blake, 1975b). It may be argued that the cilia will have a propulsive effect due to beat cycle asymmetry, as in micro-organism movement. However, the beat cycle asymmetry is far less pronounced in the muco-ciliary system (Sanderson and Sleigh, 1981) and the propulsive effect due to the cilia engaging with the highly viscous mucous layer will be an order of magnitude greater than that in the PCL. Indeed Matsui et al. (1998) showed that in the absence of a mucus layer, transport was slowed to less than 20%.

As mentioned above, we make the assumption that the mucus–PCL interface is flat throughout the beat cycle. The reasons for this are further discussed in detail in Sections 8.4 and 8.5. A consequence of this assumption is that positive propulsion necessitates penetration of the mucous layer by the cilia tips. In reality it may be possible for cilia to exert force on the mucus by 'pushing up' the mucous layer, without actually penetrating it. For all results shown in this paper, however, we assume that 'penetration' takes place. Certainly, the micrographs of Sanderson and Sleigh appear to show a nearly flat mucus–PCL interface. In addition, micrographs taken by Puchelle et al. (1998) appear to show the cilia penetrating the mucus.

4.1. The effect of the mat of cilia in the PCL—an active porous medium

The dense mat of cilia will resist the flow of fluid, somewhat like a porous medium. In addition, the cilia oscillate, so that the fluid close to the surface of a cilium will move with similar velocity as of the cilium. The combined effect is that the mat of cilia will reduce the transport of PCL, but cause significant oscillations throughout the layer. The resistive force will be assumed to act only in the PCL. This is because the cilia only penetrate the mucus for a very short portion of the cycle—at any one time, most of the volume of the mucus in the thin penetration layer will contain no cilia.

In modelling a porous medium, one can write the resistive force as being proportional to the fluid velocity, i.e. $\mathbf{f}_{\text{res}}(x, y, t) = -\gamma \mathbf{u}$, where γ is a coefficient of resistance. For our problem, the cilia are in motion, so we consider the relative motion of the fluid and the field of cilia at each point in space, so that the resistive

force is given by

$$\mathbf{f}_{\text{res}}(x, y, t) = -\gamma(\mathbf{u} - \mathbf{u}_{\text{cilia}}), \quad 0 < y < h, \tag{4}$$

following Blake (1975a).

The cilia will have both a horizontal and vertical component to their motion, and in addition the porous medium will be anisotropic—the array of cilia will have a different resistance coefficient in the x and y directions. For this problem, we use

$$\gamma_x = \frac{4\pi\mu}{\left(\log(d/r_0) - (1/2)\left(d^4 - r_0^4\right)/\left(d^4 + r_0^4\right)\right) d^2}, \tag{5}$$
$$\gamma_y = \frac{8\pi\mu}{\left(4r_0^2 - r_0^4/d^2 - 3d^2 + 4d^2\,\log(d/r_0)\right)},$$

which are the coefficients for a concentrated array of circular cylinders aligned respectively perpendicular and parallel to the flow. The parameter d is the spacing of the cilia, r_0 the radius of a cilium, log denotes the natural logarithm. This was derived in Happel (1959), and was found by Happel to compare well with experimental data. The resistance coefficients are proportional to the fluid viscosity. We use γ_x^{P}, γ_y^{P} to denote the resistance coefficients in the PCL, determined from μ^{P}, γ_x^{M1}, γ_y^{M1} to denote the resistance coefficients in the mucus, determined from μ^{M1}. The latter will be necessary when considering propulsive effects in the traction layer.

One might anticipate that the precise values of γ_x^{P}, γ_y^{P} will not be be particularly important, since throughout most of the PCL, they will be large enough so that asymptotically, $\mathbf{u} \sim \mathbf{u}_{\text{cilia}}$. This approximation was exploited in Blake (1975a) and Blake (1977), in which the motion of the cilia was more accurately represented so that propulsion due to beat cycle asymmetry, as is observed in micro-organisms, could be modelled. However, the existence of large pressure gradients in the mucociliary system may mean that the assumption $\mathbf{u} \sim \mathbf{u}_{\text{cilia}}$ may not be appropriate here. We shall see later that this is the case.

We require $\mathbf{u}_{\text{cilia}}$ as a function of (x, y, t)—we suggest a simplified Fourier series model that captures all of the important aspects of the beat cycle—periodicity, an effective stroke lasting only 20% of the duration of the total period and velocity increasing linearly with distance from the epithelium. Of course we require $\int_0^T u_{\text{cilia}}\,\mathrm{d}t = 0$, i.e. there is no net movement of any point of the cilium over a beat cycle. Hence, we use the following representation for the horizontal and vertical components of the cilium velocity:

$$u_{\text{cilia}}(x, y, t) = \nu y\sigma C(kx + \sigma t) = \nu y\sigma \left(\sum_{n=1}^{N_0} c_n \cos[(kx + \sigma t)n]\right), \tag{6}$$
$$v_{\text{cilia}}(x, y, t) = \nu y\sigma D(kx + \sigma t) = \nu y\sigma \left(\sum_{n=1}^{N_0} d_n \sin[(kx + \sigma t)n]\right).$$

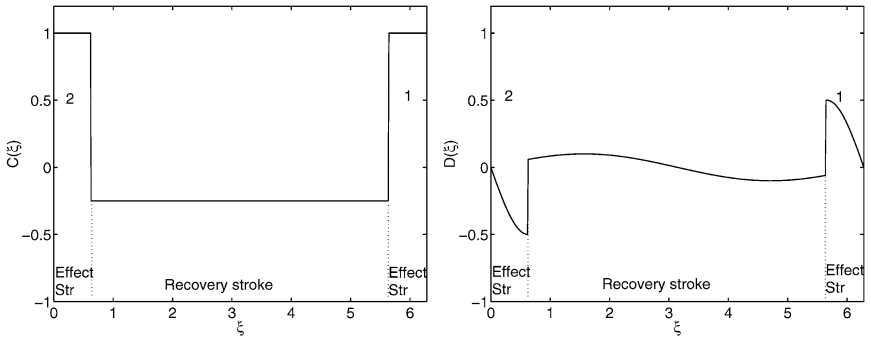

Fig. 3 Horizontal and vertical cilium tip velocity-idealised representation. See text for further details.

The parameter k is the wavenumber $2\pi/\lambda$, where λ is the wavelength, σ is the cilia beat frequency in radians per second, ν is the duration of the cilia beat as a fraction of the duration of the effective stroke. The functions C and D are shown in Fig. 3. To obtain the Fourier series coefficients, we Fourier analysed the functions C and D shown in Fig. 3, which provide a reasonable model of the velocity of the cilium, using the idea that it is approximately a pendulum moving through an arc of $\pi/3$ rad, with the effective stroke five times faster than the recovery stroke. The period denoted 1 represents the cilium beating forwards during the first half of the effective stroke, the cilium tip moving upwards into the mucus. Hence, the horizontal velocity is positive, the vertical velocity is positive, although falls to zero as the cilium tip approaches its apex. The period denoted 2 represents the cilium tip during the second half of the effective stroke, during which the cilium tip continues to beat forward, but now has negative vertical velocity until it reaches the end of the effective stroke and stops. A satisfactory representation is given by taking the first four and seven terms of the Fourier series respectively, as shown in Fig. 4. For this paper, in which we require $N_0 = 15$ terms for the solution, we set $c_5 = \cdots = c_{15} = 0 = d_8 = \cdots = d_{15}$. The values of the Fourier coefficients are given in Appendix A.

The cilium moves through an angle of about $\pi/3$ rad in one-fifth of the beat cycle, its tip covering a distance of $L\pi/3$. Assuming an angular frequency of 60 rad s^{-1}, the duration of the effective stroke is $2\pi/(60 \times 5)$ s. The velocity of the cilium tip during the effective stroke is therefore approximately

$$\nu L\sigma = \frac{L\pi/3}{2\pi/(60 \times 5)} = \frac{5\sigma L}{6}, \tag{7}$$

so $\nu = 5/6$. We assume that the vertical component of the velocity varies between 0 and $0.5\sin(\pi/6)$ of that of the horizontal velocity.

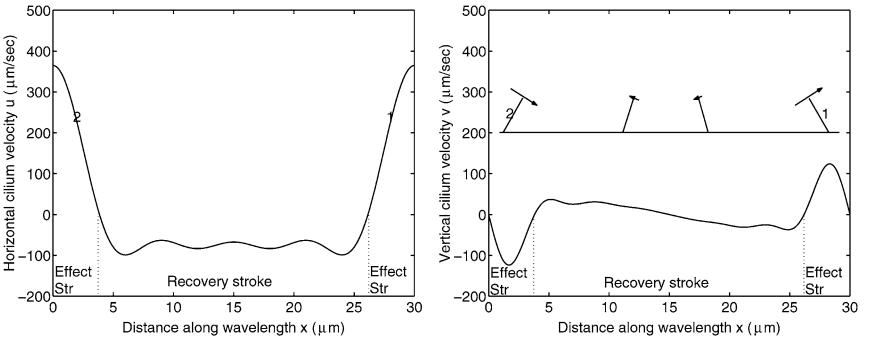

Fig. 4 Horizontal and vertical cilium tip velocity-dimensional Fourier series, with parameters $L = 6\ \mu$m, $k = 2\pi/30\ \mu\text{m}^{-1}$, $\sigma = 60\ \text{rad}\,\text{s}^{-1}$, using four and seven terms respectively in the Fourier expansion as discussed in text.

4.2. Traction layer force

A similar idea to that described above can be used to model the propulsive force produced by the cilia penetrating the mucous layer. At the level of the interface, where there will be many cilia bodies in the mucous layer, we apply the porous medium model and write the force as $\mathbf{f}_{\text{prop}} = (f_{\text{prop}}, 0, g_{\text{prop}})$, where

$$f_{\text{prop}}(x, y = h, t) = \left(\frac{1}{2} f_0 + \sum_{n=1}^{N_1} f_n \cos[(kx + \sigma t)n]\right) \gamma_x^{\text{M1}}(u - u_{\text{cilia}}), \tag{8}$$

$$g_{\text{prop}}(x, y = h, t) = \left(\sum_{n=1}^{N_1} g_n \sin[(kx + \sigma t)n]\right) \gamma_y^{\text{M1}}(v - v_{\text{cilia}}).$$

γ_x^{M1} γ_y^{M1} are resistance coefficients such as those chosen in the last section, and we choose $N_1 = 15$.

For mathematical simplicity, we simplify the interaction velocities $(u - u_{\text{cilia}})$ and $(v - v_{\text{cilia}})$ by the constants $-U_{\text{int}}$ and $-V_{\text{int}}$, making the assumption that they do not vary greatly with x or t in this small region. These constants are determined from an initial estimate and upper and lower bounds, using an iterative procedure. This is explained in more detail in Section 10.

At a level between $y = h$ and $y = L$ fewer cilia will be present, at any point in time, since the cilium tip only reaches the top of the traction layer for a brief fraction of the cycle. Above $y = L$, there will be no cilia at all. The viscous coupling between the cilia and the mucus is therefore much weaker. Hence, we assume that the force exerted by the cilia on the mucus falls monotonically to zero between $y = h$ and $y = L$. Modelling this variation by the function $\sin(\pi y/L)/\sin(\pi h/L)$

we have

$$f_{\text{prop}}(x, y, t) = -\left(\frac{1}{2} f_0 + \sum_{n=1}^{N_1} f_n \cos[(kx + \sigma t)n]\right) \gamma_x^{\text{M1}} U_{\text{int}} \frac{\sin(\pi y/L)}{\sin(\pi h/L)}, \quad (9)$$

$$g_{\text{prop}}(x, y, t) = -\left(\sum_{n=1}^{N_1} g_n \sin[(kx + \sigma t)n]\right) \gamma_y^{\text{M1}} V_{\text{int}} \frac{\sin(\pi y/L)}{\sin(\pi h/L)}.$$

We have investigated a model with the function $\sin(\pi y/L)/\sin(\pi h/L)$ replaced by a linear function, and the results are very similar.

This approach to modelling the force is not ideal, since in reality there will be complex interactions between the tips of the penetrating cilia and the mucus–PCL interface. The interface will not be a smooth, flat surface: it will deform in response to the penetration of the cilia. There may be surface forces, and there may be molecular level interactions between the 'crown' on the tip of the cilium (Puchelle et al., 1987) and the mucus polymer network. We essentially model the interface as moving closely with the penetrating cilia tips, then make a phenomenological estimate for the force in the rest of the traction layer.

The Fourier coefficients f_n are chosen by Fourier–analysing the functions F and G as depicted in Fig. 5. The function F represents positive propulsion for one-fifth of the beat-cycle—based on the data of Sanderson and Sleigh (1981)—rising linearly to a maximum value, then falling linearly back to zero. The function G scales with the vertical velocity of the cilium. Visualising the cilium beat as a simple pendular motion, we see that at the apex of the stroke, the vertical velocity is zero. In front of this point, the velocity is positive, as the cilium tip is moving up, behind this point, the velocity is negative, as the cilium tip is moving downwards. The values of the coefficients f_n, g_n can be found in Appendix A, graphs of the Fourier series representations are given in Fig. 6. We shall see that the final results also exhibit this sharp oscillation.

We have assumed that there is no variation in the force in the direction perpendicular to the effective stroke (in Fig. 2 this is the direction *into* the page), which is

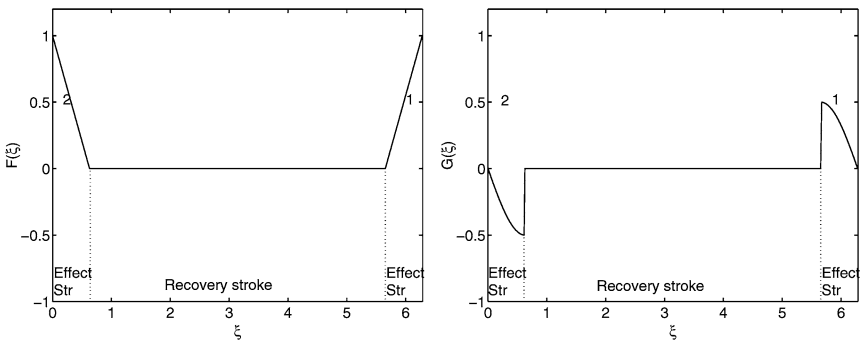

Fig. 5 Plots of the functions F and G, the idealised representations of the variations of the horizontal and vertical propulsive force in x and t.

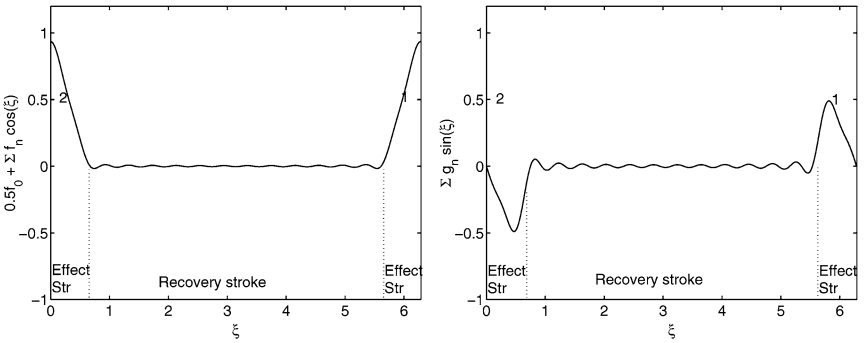

Fig. 6 Fourier series representations $0.5\,f_0 + \sum_{n=1}^{15} f_n \cos(\xi)$, $\sum_{n=1}^{15} g_n \sin(\xi)$, for $F(\xi)$, $G(\xi)$. $0 < \xi < 2\pi$.

not strictly true—in fact we have averaged over the row of cilia which we assume to be in phase. Progress towards a three-dimensional model of the flow patterns in the PCL is currently being made (Smith, 2006).

5. Constitutive relations

The next step in solving (2) is to determine relations between stress and strain. We shall consider the Newtonian PCL and non-Newtonian mucus separately.

5.1. Periciliary layer

Modelling the PCL as a Newtonian fluid, we have simply

$$\tau_{jk} = 2\mu^{\mathrm{P}} d_{jk}. \tag{10}$$

τ_{jk} is the deviatoric part of the stress tensor, so that $\sigma_{jk} = -p\delta_{jk} + \tau_{jk.}$ d_{jk} is the rate of strain tensor $(1/2)(u_{j,k} + u_{k,j})$ where commas denote differentiation.

5.2. Mucous layer

Mucus is a complex polymer gel which exhibits, amongst other behaviours, shear-thinning, viscoelasticity, spinnability and adhesiveness (Puchelle et al., 1987). A detailed review of the composition, molecular structure and rheologic properties of mucus may be found in Sleigh et al. (1988). There exists a plethora of experimental results, with varying applicability to the *in vivo* system, due to differing experimental methods, mucus collection and storage techniques and variation within and between individuals. It is also difficult to obtain uncontaminated and undisturbed mucus from the respiratory tract. Nor it is straightforward to determine how experiments should be interpreted, since only a rather complex rheological model—like that in Quemada (1984)—could be fitted to a whole spectrum of experimental results. In addition, it seems likely that, due to the varying strain rates,

the rheological properties throughout the volume of the mucus are non-uniform with, for instance, lower viscosity near the zone of ciliary penetration. It will be necessary to find a constitutive equation with an appropriate choice of parameters that provides a good representation of the relevant properties of mucus in the muco-ciliary system.

Previous experimental studies have concluded that viscoelasticity is one of the most crucial elements of the system for effective transport to occur. Meyer and Silberberg (1980) discuss how '... during the very brief period of the power stroke ... the mucous layer must react elastically, i.e. with minimum relative slip. Then, over the beginning of the recovery stroke, a period of sufficient length must again be granted for the cilium to release itself from the contact of the mucus ....' Hence, we model mucus with an elastic component which allows it to deform and then recoil in response to penetration. For analytic simplicity we choose the Maxwell constitutive equation

$$\lambda_1 \frac{\delta \tau_{jk}}{\delta t} + \tau_{jk} = 2\mu^{\mathrm{M}} d_{jk}, \tag{11}$$

with a single relaxation time λ_1 and a steady flow viscosity μ^{M}. $\delta/\delta t$ is a time derivative which is invariant under change of coordinates.

If we assume that penetration of the cilia into the mucus is small, we can make the linearisation

$$\lambda_1 \frac{\partial \tau_{jk}}{\partial t} + \tau_{jk} = 2\mu^{\mathrm{M}} d_{jk}. \tag{12}$$

In fact, mucus will possess a spectrum of relaxation mechanisms up to possibly 60 s, due to varying lengths of polymer chains and different mechanisms by which the molecular network can deform (Silberberg, 1983). A more complete model would involve a number of Maxwell elements, but since we shall restrict our attention to very short-lived deformations, we argue that one mechanism will provide a good representation. This model does not entail behaviours such as shear thinning and so we shall have to choose viscosity values appropriate to the shear stresses observed in the muco-ciliary system.

Three different classes of experiments have been performed on mucus samples: steady shearing tests, creep tests and oscillatory tests. Steady shearing tests do not represent the dynamic conditions found in the lung, and permanently destroy the structure of the mucus sample (Davis and Dippy, 1969; Reid, 1973). Creep tests give information on the time-dependent response of mucus, but are less suitable for short timescale behaviour (Fung, 1993). Oscillatory testing provides the most useful information. Two constants are found: G', the storage modulus (associated with elasticity) and G'', the loss modulus (associated with viscosity). Fung (1993) describes how these constants can be related to our constitutive equation. The strain on the mucus will be of the form $\gamma = \gamma_0 \mathrm{e}^{\mathrm{i}\omega t}$. For small oscillations the stress will respond sinusoidally, with a phase difference δ: $\tau = \tau_0 \mathrm{e}^{\mathrm{i}(\omega t+\delta)}$. Then $G^* = G' + iG'' := \tau/\gamma$. Noting that $\dot{\tau} = \mathrm{i}\omega\tau$ and $\dot{\gamma} = \mathrm{i}\omega\gamma$ we can substitute into Maxwell's

constitutive equation to show that

$$G' = \frac{\mu^{\mathrm{M}}\omega^2\lambda_1}{1+\omega^2\lambda_1^2}, \qquad G'' = \frac{\mu^{\mathrm{M}}\omega}{1+\omega^2\lambda_1^2}. \tag{13}$$

As discussed above, a set of values for G' and G'' measured over a wide rage of ω will lead to a widely varying set of values for μ^{M} and λ_1. We cannot fit the simple Maxwell model to a range of real experimental results. However, if we choose a characteristic frequency of the system, 5–10 Hz, we can find appropriate values for μ^{M} and λ_1. In this study, we use the results published by Lutz et al. (1973) for canine tracheal mucus. At the frequency of 7.2497 Hz they reported values of $G' = 1$ Pa and $G'' = 0.64491$ Pa, which correspond to the parameters $\lambda = 0.034\ \mathrm{s}^{-1}$ and $\mu^{\mathrm{M}} = 0.0482\ \mathrm{N\,m}^{-2}$ s. Since $\mu^{\mathrm{P}} \approx \mu^{\mathrm{water}} \approx 0.001\ \mathrm{N\,m}^{-2}$ s, we have $\mu^{\mathrm{M}}/\mu^{\mathrm{water}} = 48.2$.

6. Fourier series solution

Due to the periodicity of the ciliary beat, the force terms that drive the system are periodic. In addition, since we are testing the hypotonic defensin (impermeable epithelium) hypothesis, we take the boundary conditions on the epithelium to be constant, $\mathbf{u} = 0$. Neglecting airflows, the boundary conditions on the surface will also be homogeneous. Finally, we neglect any steady pressure gradient, because in the circular transport experiments of Matsui et al. (1998), no such pressure gradients could have been present, due to the fact that any such pressure must be continuous moving around one complete circle. Hence, we assume that the solution $\mathbf{u}$, p is periodic.

Writing all variables as Fourier series we have for example,

$$\tau_{jk} = \frac{(\tau_{jk})_0}{2} + \sum_{n=1}^{N} (\tau_{jk})_n, \tag{14}$$

where for $n \geq 1$, $(\tau_{jk})_n = a_n(y)\cos[n(kx+\sigma t)] + b_n(y)\sin[n(kx+\sigma t)]$, so that each $(\tau_{jk})_n$ is $2\pi/kn$-periodic in $x + \sigma t/2\pi$. The term $(\tau_{jk})_0$ is independent of both x and t. k is the wavenumber of the metachronal wave, $2\pi/\lambda$, where λ is the wavelength.

It is then possible to equate terms with periodicity in $2\pi/kn$ (and the terms constant in x and t). By writing $(\tau_{jk})_n = \mathrm{Rl}\{(\hat{\tau}_{jk})_n \mathrm{e}^{\mathrm{i}n\sigma t}\}$ (hats being used with other variables analogously, Rl denoting real part) we convert from the 'time domain' to the 'frequency domain,' in which the independent variable t is replaced by the frequency $n\sigma$. This results in a linear constitutive equation:

$$\mathrm{Rl}\{\lambda_1 \mathrm{i}n\sigma(\hat{\tau}_{jk})_n \mathrm{e}^{\mathrm{i}n\sigma t}\} + \mathrm{Rl}\{(\hat{\tau}_{jk})_n \mathrm{e}^{\mathrm{i}n\sigma t}\} = 2\mu^{\mathrm{M}}\mathrm{Rl}\{(\hat{d}_{jk})_n \mathrm{e}^{\mathrm{i}n\sigma t}\}, \tag{15}$$

which leads to

$$(\hat{\tau}_{jk})_n = \frac{2\mu^{\mathrm{M}}}{1 + \mathrm{i}n\sigma\lambda_1}(\hat{d}_{jk})_n = \frac{2\mu^{\mathrm{M}}}{\phi_n + \mathrm{i}\psi_n}(\hat{d}_{jk})_n, \tag{16}$$

where $\phi_n = 1$, $\psi_n = n\sigma\lambda_1$.

For the steady term ($n = 0$), we have the Newtonian constitutive equation

$$(\hat{\tau}_{jk})_0 = 2\mu^{\mathrm{M}}(\hat{d}_{jk})_0. \tag{17}$$

7. Fluid flow equations

The subscripts are omitted in what follows, so that for instance $\mathbf{u}_n$ is written as $\mathbf{u}$.

7.1. *Steady terms* ($n = 0$)

In all three layers we have the Newtonian constitutive equations $\hat{\tau}_{jk} = 2\mu\hat{d}_{jk}$, for μ^{P}, μ^{M1}, μ^{M2}. This leads, with Eq. (2), to the familiar Stokes flow equations:

$$\nabla\hat{p} = \mu\nabla^2\hat{\mathbf{u}} + \hat{\mathbf{f}}. \tag{18}$$

Using the fact that $\hat{p}$, $\hat{\mathbf{u}}$ are constant in x_1, we have

$$\begin{aligned} 0 &= \mu\hat{u}_{1,33} + \hat{f}_1, \\ \hat{p}_{,3} &= \mu\hat{u}_{3,33} + \hat{f}_3. \end{aligned} \tag{19}$$

We shall see later that the vertical pressure gradient will also be zero.

7.2. *Unsteady terms* ($n \geqslant 1$)

The transformed momentum equations are

$$\begin{aligned} -\hat{p}_{,1} + \hat{\tau}_{11,1} + \hat{\tau}_{13,3} + \hat{f}_1 &= 0, \\ \hat{\tau}_{31,1} + \hat{\tau}_{33,3} - \hat{p}_{,3} + \hat{f}_3 &= 0. \end{aligned} \tag{20}$$

In the mucous layers, the stress is given by Eq. (16), so

$$\begin{aligned} -\hat{p}_{,1} + 2\mu^{\mathrm{M}}(\phi + \mathrm{i}\psi)^{-1}(\hat{d}_{11,1} + \hat{d}_{13,3}) + \hat{f}_1 &= 0, \\ 2\mu^{M}(\phi + \mathrm{i}\psi)^{-1}(\hat{d}_{31,1} + \hat{d}_{33,3}) - \hat{p}_{,3} + \hat{f}_3 &= 0. \end{aligned} \tag{21}$$

Using the continuity equation this simplifies to, in vector notation

$$\nabla \hat{p} = \frac{\mu^{\mathrm{M}}}{\phi + i\psi}\nabla^2 \hat{\mathbf{u}} + \hat{\mathbf{f}}, \tag{22}$$

which we recognise as the Stokes flow momentum equation with complex viscosity $\mu^{\mathrm{M}}/(\phi + i\psi)$. Similarly, in the PCL we have

$$\nabla \hat{p} = \mu^{\mathrm{P}}\ \nabla^2 \hat{\mathbf{u}} + \hat{\mathbf{f}}. \tag{23}$$

7.3. Force terms

To simplify the notation we replace u_1, u_3, x_1, x_3, f_1 and f_3 with u, v, x, y, f and g, respectively. As before, we omit subscripts to denote the term in the Fourier series for the force, velocity and pressure. In the PCL the force terms are, for $n \geqslant 0$,

$$\begin{aligned} f &= -\gamma_x^{\mathrm{P}}(u - \nu y \sigma c_n \cos((kx + \sigma t)n), \\ g &= -\gamma_y^{\mathrm{P}}(v - \nu y \sigma d_n \sin((kx + \sigma t)n). \end{aligned} \tag{24}$$

Writing $u = \mathrm{Rl}\{(\check{u}^{\mathrm{r}} + \mathrm{i}\check{u}^{\mathrm{i}})\mathrm{e}^{in(kx+\sigma t)}\}$, and similarly for other variables we have

$$\begin{aligned} &\check{f}^{\mathrm{r}} = -\gamma_x^{\mathrm{P}}(\check{u}^{\mathrm{r}} - \nu y \sigma c_n), \qquad \check{f}^{\mathrm{i}} = -\gamma_x^{\mathrm{P}}\check{u}^{\mathrm{i}}, \\ &\check{g}^{\mathrm{i}} = -\gamma_y^{\mathrm{P}}(\check{v}^{\mathrm{i}} + \nu y \sigma d_n), \qquad \check{g}^{\mathrm{r}} = -\gamma_y^{\mathrm{P}}\check{v}^{\mathrm{r}}, \qquad 0 < y < h. \end{aligned} \tag{25}$$

In the traction layer the force terms are

$$\begin{aligned} &\check{f}^{\mathrm{r}} = -U_{\mathrm{int}}\gamma_x^{\mathrm{M1}} f_n \frac{\sin(\pi y/L)}{\sin(\pi h/L)}, \qquad \check{f}^{\mathrm{i}} = 0, \\ &\check{g}^{\mathrm{i}} = V_{\mathrm{int}}\gamma_y^{\mathrm{M1}} g_n \frac{\sin(\pi y/L)}{\sin(\pi h/L)}, \qquad \check{g}^{\mathrm{r}} = 0 \qquad (h < y < L). \end{aligned} \tag{26}$$

8. Field equations and boundary conditions

8.1. Field equations in the PCL

We nondimensionalise as follows: $x = \lambda x'$, $y = Ly'$, $u = \sigma L u'$, $v = (\sigma L^2/\lambda)v'$, $p = \mathcal{P}^{\mathrm{P}} p'$, $f = (\mu^{\mathrm{P}}\sigma/L) f'$. The scaling for v ensures that the continuity equation is balanced. For convenience we omit the primes. We shall also use h and H to represent the nondimensional parameters h/L and H/L. The terms $\hat{\mathbf{u}}$, $\hat{p}$ are now $1/n$-periodic in $2\pi x$. In addition, we write θ_1 and θ_2 for the viscosity ratios $\mu^{\mathrm{M1}}/\mu^{\mathrm{P}}$ and

μ^{M2}/μ^{M1}, respectively. Then for $n = 0$,

$$\begin{aligned} 0 &= \frac{\sigma\mu^{P}}{L}\frac{d^2\hat{u}}{dy^2} + \frac{\mu^{P}\sigma}{L}\hat{f}, \\ \frac{\mathcal{P}^{P}}{L}\frac{d\hat{p}}{dy} &= \frac{\sigma}{\lambda}\mu^{P}\frac{d^2\hat{v}}{dy^2} + \frac{\mu^{P}\sigma}{L}\hat{g}, \end{aligned} \tag{27}$$

and for $n \geqslant 1$,

$$\begin{aligned} \frac{\mathcal{P}^{P}}{\lambda}\frac{\partial\hat{p}}{\partial x} &= \sigma L\mu^{P}\left(\frac{1}{\lambda^2}\frac{\partial^2\hat{u}}{\partial x^2} + \frac{1}{L^2}\frac{\partial^2\hat{u}}{\partial y^2}\right) + \frac{\mu^{P}\sigma}{L}\hat{f}, \\ \frac{\mathcal{P}^{P}}{L}\frac{\partial\hat{p}}{\partial y} &= \frac{\sigma L^2}{\lambda}\mu^{P}\left(\frac{1}{\lambda^2}\frac{\partial^2\hat{v}}{\partial x^2} + \frac{1}{L^2}\frac{\partial^2\hat{v}}{\partial y^2}\right) + \frac{\mu^{P}\sigma}{L}\hat{g}. \end{aligned} \tag{28}$$

For $n = 0$, $\partial\hat{u}/\partial x = 0$, so by the continuity equation $\partial\hat{v}/\partial y = 0$. As discussed above, $\hat{v} = 0$ on $y = 0$ so $\hat{v} \equiv 0$ for all y. Since the zeroth term of the vertical force $\hat{g} = 0$, the second equation is then simply $\partial\hat{p}/\partial y = 0$, and so the pressure is constant. Hence

$$0 = \frac{d^2\hat{u}}{dy^2} + \hat{f}. \tag{29}$$

For $n \geqslant 1$, in order to balance the first equation we choose the pressure scaling $\mathcal{P}^{P} = \mu^{P}\sigma\lambda/L$. Hence

$$\frac{\partial\hat{p}}{\partial x} = \frac{L^2}{\lambda^2}\frac{\partial^2\hat{u}}{\partial x^2} + \frac{\partial^2\hat{u}}{\partial y^2} + \hat{f}, \tag{30}$$

$$\frac{\partial\hat{p}}{\partial y} = \frac{L^4}{\lambda^4}\frac{\partial^2\hat{v}}{\partial x^2} + \frac{L^2}{\lambda^2}\frac{\partial^2\hat{v}}{\partial y^2} + \frac{L}{\lambda}\hat{g}. \tag{31}$$

It may appear that it is possible to apply lubrication theory, by noting that $L^2/\lambda^2 \ll 1$. However, the Fourier series representation of u means that $\hat{u} = (\check{u}^{r} + i\check{u}^{i})e^{2\pi nxi}$, so that $\partial^2\hat{u}/\partial x^2 = -4\pi^2n^2\hat{u}$. Using this representation, we can rewrite the real and imaginary parts of the $n \geqslant 1$ equations as

$$\begin{aligned} -2\pi n\check{p}^{i} &= -\chi^2\hat{u}^{r} + \frac{d^2\check{u}^{r}}{dy^2} + \check{f}^{r}, \\ 2\pi n\check{p}^{r} &= -\chi^2\hat{u}^{i} + \frac{d^2\check{u}^{i}}{dy^2} + \check{f}^{i}, \\ \frac{d\check{p}^{r}}{dy} &= -\chi^2\varepsilon^2\check{v}^{r} + \varepsilon^2\frac{d^2\check{v}^{r}}{dy^2} + \varepsilon\check{g}^{r}, \\ \frac{d\check{p}^{i}}{dy} &= -\chi^2\varepsilon^2\check{v}^{i} + \varepsilon^2\frac{d^2\check{v}^{i}}{dy^2} + \varepsilon\check{g}^{i}, \end{aligned} \tag{32}$$

where $\varepsilon = L/\lambda$ and $\chi = 2\pi n\varepsilon$. Using the scaling $\mu^{\mathrm{P}}\sigma/L$ for the force terms and using Eq. (25), we have for $n = 0$,

$$0 = \frac{\mathrm{d}^2\breve{u}^{r,i}}{\mathrm{d}y^2} - \alpha_x^2\breve{u}^{\mathrm{r,i}}, \tag{33}$$

and for $n \geqslant 1$,

$$\begin{aligned}
-2\pi n\breve{p}^{\mathrm{i}} &= -\beta_x^2\breve{u}^{\mathrm{r}} + \frac{\mathrm{d}^2\breve{u}^{r}}{\mathrm{d}y^2} + \nu y c_n\alpha_x^2,\\
2\pi n\breve{p}^{\mathrm{r}} &= -\beta_x^2\breve{u}^{\mathrm{i}} + \frac{\mathrm{d}^2\breve{u}^{i}}{\mathrm{d}y^2},\\
\mathrm{d}\breve{p}^{\mathrm{r}}y &= -\beta_y^2\varepsilon^2\breve{v}^{\mathrm{r}} + \varepsilon^2\frac{\mathrm{d}^2\breve{u}^{r}}{\mathrm{d}y^2},\\
\mathrm{d}\breve{p}^{\mathrm{i}}y &= -\beta_y^2\varepsilon^2\breve{v}^{\mathrm{i}} + \varepsilon^2\frac{\mathrm{d}^2\breve{u}^{i}}{\mathrm{d}y^2} - \varepsilon\nu y d_n\alpha_y^2,
\end{aligned} \tag{34}$$

where the resistance parameters are defined as $\alpha_x^2 = \gamma_x^{\mathrm{P}}L^2/\mu^{\mathrm{P}}$, $\alpha_y^2 = \gamma_y^{\mathrm{P}}L^2/\mu^{\mathrm{P}}$, $\beta_x^2 = \chi^2 + \alpha_x^2$, $\beta_y^2 = \chi^2 + \alpha_y^2$. Note that α_x, α_y are independent of the value of the viscosity, and so also apply in the mucous layer.

8.2. Field equations in the mucus

After nondimensionalising we have for $n = 0$,

$$\begin{aligned}
0 &= \frac{\sigma\mu^{\mathrm{M}}}{L}\frac{\mathrm{d}^2\hat{u}}{\mathrm{d}y^2} + \frac{\mu^{\mathrm{M}}\sigma}{L}\hat{f},\\
\frac{\mathcal{P}^{\mathrm{M}}}{L}\frac{\mathrm{d}\hat{p}}{\mathrm{d}y} &= \frac{\sigma\mu^{\mathrm{M}}}{\lambda}\frac{\mathrm{d}^2\hat{v}}{\mathrm{d}y^2} + \frac{\mu^{\mathrm{M}}\sigma}{L}\hat{g},
\end{aligned} \tag{35}$$

and for $n \geqslant 1$,

$$\begin{aligned}
\frac{\mathcal{P}^{\mathrm{M}}}{\lambda}\frac{\partial\hat{p}}{\partial x} &= \frac{\sigma L\mu^{\mathrm{M}}}{\phi + \mathrm{i}\psi}\left(\frac{-4\pi^2n^2}{\lambda^2}\hat{u} + \frac{1}{L^2}\frac{\partial^2\hat{u}}{\partial y^2}\right) + \frac{\mu^{\mathrm{M}}\sigma}{L}\hat{f},\\
\frac{\mathcal{P}^{\mathrm{M}}}{L}\frac{\partial\hat{p}}{\partial y} &= \frac{\sigma L^2\mu^{\mathrm{M}}}{\lambda(\phi + \mathrm{i}\psi)}\left(\frac{-4\pi^2n^2}{\lambda^2}\hat{v} + \frac{1}{L^2}\frac{\partial^2\hat{v}}{\partial y^2}\right) + \frac{\mu^{\mathrm{M}}\sigma}{L}\hat{g}.
\end{aligned} \tag{36}$$

As before, for $n = 0$, $\hat{v} \equiv 0$ so the velocity can be found from Eq. (29). For $n \geqslant 1$, in order to balance the first equation we choose the pressure scaling $\mathcal{P}^{\mathrm{M}} =$

$\mu^{\mathrm{M}}\sigma\lambda/(L[\phi+\mathrm{i}\psi])$, so

$$\frac{\partial\hat{p}}{\partial x}=\left(\frac{-4\pi^2n^2L^2}{\lambda^2}\hat{u}+\frac{\partial^2\hat{u}}{\partial y^2}\right)+(\phi+\mathrm{i}\psi)\hat{f},$$
$$\frac{\partial\hat{p}}{\partial y}=\left(\frac{-4\pi^2n^2L^4}{\lambda^4}\hat{v}+\frac{L^2}{\lambda^2}\frac{\partial^2\hat{v}}{\partial y^2}\right)+\frac{L(\phi+\mathrm{i}\psi)}{\lambda}\hat{g}. \tag{37}$$

For $n=0$, $\hat{p}$ is constant, which may be taken to be zero, so that the first equation is solved to give $\hat{u}$, then the continuity equation gives $\hat{v}\equiv 0$. Decomposing variables as previously we note that in terms of nondimensional variables,

$$\check{f}^{\mathrm{r}}=-\frac{L}{\mu^{\mathrm{M1}}\sigma}\sigma LU_{\mathrm{int}}f_n\gamma_x^{\mathrm{M1}}\frac{\sin(\pi y)}{\sin(\pi h)},\qquad \check{f}^{\mathrm{i}}=0,$$
$$\check{g}^{\mathrm{i}}=\frac{L}{\mu^{\mathrm{M1}}\sigma}\frac{\sigma L^2}{\lambda}V_{\mathrm{int}}g_n\gamma_y^{\mathrm{M1}}\frac{\sin(\pi y)}{\sin(\pi h)},\qquad \check{g}^{\mathrm{r}}=0. \tag{38}$$

Hence we have, in the traction layer $h<y<1$ for $n=0$,

$$0=\frac{\mathrm{d}^2\check{u}^{\mathrm{r}}}{\mathrm{d}y^2}-f_0\alpha_x^2U_{\mathrm{int}}\frac{\sin(\pi y)}{\sin(\pi h)},\qquad 0=\frac{\mathrm{d}^2\check{u}^{\mathrm{i}}}{\mathrm{d}y^2}\qquad (n=0) \tag{39}$$

and for $n\geq 1$,

$$-2\pi n\check{p}^{\mathrm{i}}=-\chi^2\check{u}^{\mathrm{r}}+\frac{\mathrm{d}^2\check{u}^{\mathrm{r}}}{\mathrm{d}y^2}-\phi f_n\alpha_x^2U_{\mathrm{int}}\frac{\sin(\pi y)}{\sin(\pi h)},$$
$$2\pi n\check{p}^{\mathrm{r}}=-\chi^2\check{u}^{\mathrm{i}}+\frac{\mathrm{d}^2\check{u}^{\mathrm{i}}}{\mathrm{d}y^2}-\psi f_n\alpha_x^2U_{\mathrm{int}}\frac{\sin(\pi y)}{\sin(\pi h)},$$
$$\mathrm{d}\check{p}^{\mathrm{r}}y=-\chi^2\varepsilon^2\check{v}^{\mathrm{r}}+\varepsilon^2\frac{\mathrm{d}^2\check{v}^{\mathrm{r}}}{\mathrm{d}y^2}-\varepsilon\psi g_n\alpha_y^2V_{\mathrm{int}}\frac{\sin(\pi y)}{\sin(\pi h)},$$
$$\mathrm{d}\check{p}^{\mathrm{i}}y=-\chi^2\varepsilon^2\check{v}^{\mathrm{i}}+\varepsilon^2\frac{\mathrm{d}^2\check{v}^{\mathrm{i}}}{\mathrm{d}y^2}+\varepsilon\phi g_n\alpha_y^2V_{\mathrm{int}}\frac{\sin(\pi y)}{\sin(\pi h)}\qquad (n\geqslant 1) \tag{40}$$

In the force-free mucous layer $1<y<H$, the fluid flow equations are given by replacing f_n, g_n with zero in Eqs. (39) and (40)

8.3. Continuity equation

The continuity equation takes the same form in all three layers. As discussed above, for $n=0$, $\partial u/\partial x=0$, so $v\equiv 0$. For $n\geqslant 1$

$$-2\pi n\check{u}^{\mathrm{i}}+\frac{\mathrm{d}\check{v}^{r}}{\mathrm{d}y}=0,\qquad 2\pi n\check{u}^{\mathrm{r}}+\frac{\mathrm{d}\check{v}^{i}}{\mathrm{d}y}=0. \tag{41}$$

To solve the system it will be convenient to differentiate these equations with respect to y,

$$-2\pi n\frac{\mathrm{d}\check{u}^i}{\mathrm{d}y}+\frac{\mathrm{d}^2\check{v}^r}{\mathrm{d}y^2}=0,\qquad 2\pi n\frac{\mathrm{d}\check{u}^r}{\mathrm{d}y}+\frac{\mathrm{d}^2\check{v}^i}{\mathrm{d}y^2}=0. \tag{42}$$

If we impose these conditions in each layer, along with the original mass conservation equation on a boundary and the interfaces, mass conservation will hold throughout the fluid.

8.4. Surface and interface tension

Surface tension forces will act on the mucus–air interface, and possibly at the interface between the mucus and PCL. By considering the surface as $\eta = H + \varepsilon\cos(kx+\sigma t)$ and approximating the curvature as $|\eta_{xx}| = \mathrm{O}(4\pi^2\varepsilon/\lambda^2)$, and by approximating the surface stress as $|\mu\eta_t/L| = \mathrm{O}(\mu\varepsilon\sigma/L)$, we have the following estimate for the capillary number, the ratio of the magnitudes of surface tension to viscous forces,

$$\mathcal{C} = \mathrm{O}\left(\frac{\lambda^2\mu^{\mathrm{M2}}\sigma}{4\pi^2\mathcal{T}L}\right). \tag{43}$$

This is similar to the dimensionless number found by Ross (1971), only with an additional factor of $4\pi^2$.

Albers et al. (1996) determined values of surface tension of sputum for patients with cystic fibrosis and chronic bronchitis, comparing two different methods. The means for each condition and each method lay between 72 and 93 dyne cm^{-1}, so we estimate mucus surface tension by 80 dyne cm^{-1}, or 0.08N m^{-1} in SI units. Using the formula of Ross with the additional factor of $4\pi^2$, and parameters in SI units, $\mathcal{T} = 0.08$, $L = 6\times10^{-6}$, $\lambda = 3\times10^{-5}$, $\mu^{\mathrm{M2}} = 0.0482$ and $\sigma = 60$ we have $C = 1/7300$. This shows that surface tension forces will flatten the surface on a timescale much shorter than the ciliary beat duration, and explains why in the micrographs of Sanderson and Sleigh (1981), the mucus surface is remarkably flat, despite the rapid oscillations in velocity below. It is therefore reasonable to assume that surface tension flattens both the mucus surface and the mucus–PCL interface on a timescale much faster than the ciliary beat. We shall take the mucus–PCL interface to be a flat surface given by $y = h$ and the mucus surface to be given by $y = H$. The system will be solved with boundary conditions of zero normal velocity. This is discussed briefly in Sections 11.4 and 11.6. Future modelling may address the effect of small perturbations to the interface and surface, and the interaction between such instabilities and the viscoelastic properties of the fluid.

8.5. Traction layer mucus–PCL interface

Because we do not explicitly model the action of interface tension, it is not possible to calculate the normal stress balance on the interface. Instead we use the boundary condition of zero vertical velocity. Together with continuity of tangential stress

we have, in tensor notation

$$\tau_{13}^{\mathrm{P}} = \tau_{13}^{\mathrm{M1}}, \qquad u_3^{\mathrm{M1}} = 0. \tag{44}$$

Making the transformation to the frequency domain this becomes

$$\begin{aligned}
\mu^{\mathrm{P}}\big(\hat{u}_{1,3}^{\mathrm{P}} + \hat{u}_{3,1}^{\mathrm{P}}\big) &= \mu^{\mathrm{M1}}\big(\hat{u}_{1,3}^{M} + \hat{u}_{3,1}^{M}\big), \qquad \hat{u}_3^{\mathrm{M1}} = 0 \qquad (n=0),\\
\mu^{\mathrm{P}}\big(\hat{u}_{1,3}^{\mathrm{P}} + \hat{u}_{3,1}^{\mathrm{P}}\big) &= \mu^{\mathrm{M1}}(\phi_n + i\,\psi_n)^{-1}\big(\hat{u}_{1,3}^{M} + \hat{u}_{3,1}^{M}\big), \qquad \hat{u}_3^{\mathrm{M1}} = 0 \quad (n \geqslant 1).
\end{aligned} \tag{45}$$

Nondimensionalising we have

$$\begin{aligned}
\big(\hat{u}_{1,3}^{\mathrm{P}} + \varepsilon^2\hat{u}_{3,1}^{\mathrm{P}}\big) &= \theta_1\big(\hat{u}_{1,3}^{\mathrm{M1}} + \varepsilon^2\hat{u}_{3,1}^{\mathrm{M1}}\big), \qquad \hat{u}_3^{\mathrm{M1}} = 0 \qquad (n=0),\\
(\phi + \mathrm{i}\psi)\big(\hat{u}_{1,3}^{\mathrm{P}} + \varepsilon^2\hat{u}_{3,1}^{\mathrm{P}}\big) &= \theta_1\big(\hat{u}_{1,3}^{\mathrm{M1}} + \varepsilon^2\hat{u}_{3,1}^{\mathrm{M1}}\big), \qquad \hat{u}_3^{\mathrm{M1}} = 0 \quad (n \geqslant 1).
\end{aligned} \tag{46}$$

As discussed above, for $n = 0$, $\hat{u}_3 = 0$ and $\hat{p} = 0$. Noting that $\partial\hat{v}/\partial x = 2\pi n\mathrm{i}\hat{v}$, and writing $u_1 = u$, $u_3 = v$ as above,

$$\frac{\partial\hat{u}^{\mathrm{P}}}{\partial y} = \theta_1\frac{\partial\hat{u}^{\mathrm{M1}}}{\partial y}, \tag{47}$$

and for $n \geqslant 1$,

$$(\phi + \mathrm{i}\psi)\left(\frac{\partial\hat{u}^{\mathrm{P}}}{\partial y} + 2\pi n\mathrm{i}\varepsilon^2\hat{v}^{\mathrm{P}}\right) = \theta_1\left(\frac{\partial\hat{u}^{\mathrm{M1}}}{\partial y} + 2\pi n\mathrm{i}\varepsilon^2\hat{v}^{\mathrm{M1}}\right), \qquad \hat{v}^{\mathrm{M1}} = 0. \tag{48}$$

There is now only one matching condition for $n = 0$, which is appropriate since the vertical component of the momentum equation is trivially satisfied. By taking real and imaginary parts,

$$\frac{\mathrm{d}\check{u}^{\mathrm{r,i\,P}}}{\mathrm{d}y} = \theta_1\frac{\mathrm{d}\check{u}^{\mathrm{r,i\,M1}}}{\mathrm{d}y}, \tag{49}$$

and for $n \geqslant 1$,

$$\begin{aligned}
\frac{\phi}{\theta_1}\frac{\mathrm{d}\check{u}^{\mathrm{r\,P}}}{\mathrm{d}y} - \frac{\psi}{\theta_1}\frac{\mathrm{d}\check{u}^{\mathrm{i\,P}}}{\mathrm{d}y} - \frac{2\pi n\varepsilon^2}{\theta_1}\left(\phi\check{v}^{\mathrm{i\,P}} + \psi\check{v}^{\mathrm{r\,P}}\right) &= \frac{\mathrm{d}\check{u}^{\mathrm{r\,M1}}}{\mathrm{d}y} - 2\pi n\varepsilon^2\check{v}^{\mathrm{i\,M1}},\\
\frac{\phi}{\theta_1}\frac{\mathrm{d}\check{u}^{\mathrm{i\,P}}}{\mathrm{d}y} + \frac{\psi}{\theta_1}\frac{\mathrm{d}\check{u}^{\mathrm{r\,P}}}{\mathrm{d}y} + \frac{2\pi n\varepsilon^2}{\theta_1}\left(\phi\check{v}^{\mathrm{r\,P}} - \psi\check{v}^{\mathrm{i\,P}}\right) &= \frac{\mathrm{d}\check{u}^{\mathrm{i\,M1}}}{\mathrm{d}y} + 2\pi n\varepsilon^2\check{v}^{\mathrm{r\,M1}},\\
\check{v}^{\mathrm{r\,M1}} &= 0,\\
\check{v}^{\mathrm{i\,M1}} &= 0.
\end{aligned} \tag{50}$$

8.6. Upper mucus–traction layer interface

In this section we examine the 'interface' at $y = 1$ between the shear thinned traction layer subject to the propulsive force of the cilia, and the upper mucous layer free from volume forces. We assume that there is no interface tension acting since the mucus is essentially one fluid. This leaves us to consider continuity of both tangential and normal stress,

$$\tau_{13}^{\mathrm{M1}} = \tau_{13}^{\mathrm{M2}}, \qquad -p^{\mathrm{M1}} + \tau_{33}^{\mathrm{M1}} = -p^{\mathrm{M2}} + \tau_{33}^{\mathrm{M2}}. \tag{51}$$

We nondimensionalise with pressure scalings $\mathcal{P}^{\mathrm{M1}} = \mu^{\mathrm{M1}}\sigma\lambda/([\phi + \mathrm{i}\psi]L)$ and $\mathcal{P}^{\mathrm{M2}} = \mu^{\mathrm{M2}}\sigma\lambda/([\phi + \mathrm{i}\psi]L)$. Taking real and imaginary parts for $n = 0$,

$$\frac{\mathrm{d}\check{u}^{\mathrm{r\,M1}}}{\mathrm{d}y} = \theta_2 \frac{\mathrm{d}\check{u}^{\mathrm{r\,M2}}}{\mathrm{d}y}, \qquad \frac{\mathrm{d}\check{u}^{\mathrm{i\,M1}}}{\mathrm{d}y} = \theta_2 \frac{\mathrm{d}\check{u}^{\mathrm{i\,M2}}}{\mathrm{d}y}, \tag{52}$$

and for $n \geqslant 1$,

$$\begin{aligned}
\frac{\mathrm{d}\check{u}^{\mathrm{r\,M1}}}{\mathrm{d}y} - 2\pi n\varepsilon^2 \check{v}^{\mathrm{i\,M1}} &= \theta_2 \left(\frac{\mathrm{d}\check{u}^{\mathrm{r\,M2}}}{\mathrm{d}y} - 2\pi n\varepsilon^2 \check{v}^{\mathrm{i\,M2}} \right), \\
\frac{\mathrm{d}\check{u}^{\mathrm{i\,M1}}}{\mathrm{d}y} + 2\pi n\varepsilon^2 \check{v}^{\mathrm{r\,M1}} &= \theta_2 \left(\frac{\mathrm{d}\check{u}^{\mathrm{i\,M2}}}{\mathrm{d}y} + 2\pi n\varepsilon^2 \check{v}^{\mathrm{r\,M2}} \right),
\end{aligned} \tag{53}$$

$$\begin{aligned}
-\check{p}^{\mathrm{r\,M1}} + 2\varepsilon^2 \frac{\mathrm{d}\check{v}^{\mathrm{r\,M1}}}{\mathrm{d}y} &= -\theta_2 \check{p}^{\mathrm{r\,M2}} + 2\theta_2\varepsilon^2 \frac{\mathrm{d}\check{v}^{\mathrm{r\,M2}}}{\mathrm{d}y}, \\
-\check{p}^{\mathrm{i\,M1}} + 2\varepsilon^2 \frac{\mathrm{d}\check{v}^{\mathrm{i\,M1}}}{\mathrm{d}y} &= -\theta_2 \check{p}^{\mathrm{i\,M2}} + 2\theta_2\varepsilon^2 \frac{\mathrm{d}\check{v}^{\mathrm{i\,M2}}}{\mathrm{d}y}.
\end{aligned} \tag{54}$$

8.7. The mucus free surface

Neglecting the viscosity of air, supposing that the air pressure is constant, and making the assumption that the mucus surface is flat, we have for the tangential stress $\sigma_{1k}n_k = 0$ where $\mathbf{n} = (0, 0, 1)$. As for the mucus–PCL interface we replace the normal stress balance with the condition that the vertical velocity is zero. The conditions are therefore

$$\tau_{13}^{\mathrm{M2}} = 0, \qquad \hat{u}_3^{\mathrm{M2}} = 0. \tag{55}$$

These are transformed into, for $n = 0$,

$$\mu^{\mathrm{M2}}\left(\hat{u}_{1,3}^{\mathrm{M2}} + \hat{u}_{3,1}^{\mathrm{M2}}\right) = 0, \qquad \hat{u}_3^{\mathrm{M2}} = 0, \tag{56}$$

and for $n \geqslant 1$,

$$\frac{\mu^{\mathrm{M2}}}{\phi + \mathrm{i}\psi}\left(\hat{u}^{\mathrm{M2}}_{1,3} + \hat{u}^{\mathrm{M2}}_{3,1}\right) = 0, \qquad \hat{u}^{\mathrm{M2}}_{3} = 0. \tag{57}$$

Nondimensionalising as above and taking real and imaginary parts, for $n = 0$

$$\frac{\mathrm{d}\check{u}^{\mathrm{r\,M2}}}{\mathrm{d}y} = 0, \qquad \frac{\mathrm{d}\check{u}^{\mathrm{i\,M2}}}{\mathrm{d}y} = 0, \tag{58}$$

and for $n \geqslant 1$,

$$\begin{gathered}\frac{\mathrm{d}\check{u}^{\mathrm{r\,M2}}}{\mathrm{d}y} - 2\pi n\varepsilon^2 \check{v}^{\mathrm{i\,M2}} = 0, \quad \frac{\mathrm{d}\check{u}^{\mathrm{i\,M2}}}{\mathrm{d}y} + 2\pi n\varepsilon^2 \check{v}^{\mathrm{r\,M2}} = 0, \\ \check{v}^{\mathrm{r\,M2}} = 0, \quad \check{v}^{\mathrm{i\,M2}} = 0.\end{gathered} \tag{59}$$

8.8. No-slip conditions

As discussed above, we assume that there is no flow through the epithelium, so that $v = 0$ on $y = 0$ for all n. In addition, for viscous flow we have the no-slip boundary condition $u = 0$ on the solid interface at $y = 0$.

Finally, the fluid velocity will be continuous across the boundaries, so that $u^{\mathrm{P}} = u^{\mathrm{M1}}$, $v^{\mathrm{P}} = v^{\mathrm{M1}}$ on $y = h$ and $u^{\mathrm{M1}} = u^{\mathrm{M2}}$, $v^{\mathrm{M1}} = v^{\mathrm{M2}}$ on $y = 1$. For $n = 0$ we have six variables, $\check{u}^{\mathrm{r\,P}}$, $\check{u}^{\mathrm{i\,P}}$, $\check{u}^{\mathrm{r\,M1}}$, $\check{u}^{\mathrm{i\,M1}}$, $\check{u}^{\mathrm{r\,M2}}$, $\check{u}^{\mathrm{i\,M2}}$, six second-order ODEs from the u component of the momentum equations, and 12 boundary and matching conditions. The ODEs are linear with constant coefficients and so can be solved analytically.

For $n \geqslant 1$ we have additionally $\check{v}^{\mathrm{r\,P}}$, $\check{v}^{\mathrm{i\,P}}$, $\check{v}^{\mathrm{r\,M1}}$, $\check{v}^{\mathrm{i\,M1}}$, $\check{v}^{\mathrm{r\,M2}}$, $\check{v}^{\mathrm{i\,M2}}$, $\check{p}^{\mathrm{r\,P}}$, $\check{p}^{\mathrm{i\,P}}$, $\check{p}^{\mathrm{r\,M1}}$, $\check{p}^{\mathrm{i\,M1}}$, $\check{p}^{\mathrm{r\,M2}}$, $\check{p}^{\mathrm{i\,M2}}$, a total of 18 variables. By counting the first derivatives of the velocity terms as variables, we have a total of 30. There are 12 momentum equations, given in Sections 8.1 and 8.2, and 6 equations following from mass conservation, given in Section 8.3. Using the first derivatives of the velocity terms, the second order momentum equations can be rewritten as 24 first order ODEs, giving a total of 30. There are 4 no-slip boundary conditions, 8 conditions for continuity of velocity, 12 conditions for continuity of stress, given in Sections 8.5–8.7, and 6 conditions to enforce conservation of mass, as discussed in Section 8.3. This gives a total of 30 boundary and matching conditions in total, closing the system.

9. Steady flow solution

It is now possible to solve for the steady term of the fluid velocity analytically. It is easily seen that $\check{u}^{\mathrm{i}} = 0$ is the solution for the imaginary part of the momentum

equations. Hence $u = \breve{u}^{\mathrm{r}}$. We have the momentum equations

$$\begin{aligned} -\alpha^2 u^{\mathrm{P}} + \frac{\mathrm{d}^2 u^{\mathrm{P}}}{\mathrm{d}y^2} &= 0, \\ \frac{\mathrm{d}^2 u^{\mathrm{M1}}}{\mathrm{d}y^2} &= \alpha_x^2 U_{\mathrm{int}} f_0 \frac{\sin(\pi y)}{\sin(\pi h)}, \\ \frac{\mathrm{d}^2 u^{\mathrm{M2}}}{\mathrm{d}y^2} &= 0, \end{aligned} \tag{60}$$

boundary conditions,

$$u^{\mathrm{P}}(y=0) = 0, \qquad \frac{\mathrm{d}u^{\mathrm{M2}}}{\mathrm{d}y}(y=H) = 0, \tag{61}$$

and matching conditions,

$$\begin{aligned} u^{\mathrm{P}} &= u^{\mathrm{M1}}, \qquad \mu^{\mathrm{P}} \frac{\mathrm{d}u^{P}}{\mathrm{d}y} = \mu^{\mathrm{M1}} \frac{\mathrm{d}u^{\mathrm{M1}}}{\mathrm{d}y} \qquad (y=h), \\ u^{\mathrm{M1}} &= u^{\mathrm{M2}}, \qquad \mu^{\mathrm{M1}} \frac{\mathrm{d}u^{\mathrm{M1}}}{\mathrm{d}y} = \mu^{\mathrm{M2}} \frac{\mathrm{d}u^{\mathrm{M2}}}{\mathrm{d}y} \qquad (y=1). \end{aligned} \tag{62}$$

These are integrated to give the solution

$$\begin{aligned} u^{\mathrm{P}} &= -\frac{U_{\mathrm{int}} f_0 \alpha_x \theta_1 (1+\cos(\pi h)) \sinh(\alpha_x y)}{\pi \sin(\pi h) \cosh(\alpha_x h)}, \\ u^{\mathrm{M1}} &= -\frac{U_{\mathrm{int}} f_0 \alpha_x^2}{\pi \sin(\pi h)} \left\{ \frac{\theta_1}{\alpha} \tanh(\alpha_x h)(1+\cos(\pi h)) + l(y) - l(h) \right\}, \\ u^{\mathrm{M2}} &= -\frac{U_{\mathrm{int}} f_0 \alpha_x^2}{\pi \sin(\pi h)} \left\{ \frac{\theta_1}{\alpha} \tanh(\alpha_x h)(1+\cos(\pi h)) + l(1) - l(h) \right\}, \end{aligned} \tag{63}$$

where $l(y) = y + \sin(\pi y)/\pi$. The constant U_{int} is determined in Section 10, and through this the mean transport depends on the parameters λ_1 and θ_2. The solution is very simple in form—throughout the region $y > 1$, the velocity is constant. In the penetration region $h < y < 1$ the velocity is approximately linear. In the region $y < h$, the solution is approximately proportional to the exponential $\mathrm{e}^{\alpha_x(y-h)}$ in a region of size $\mathrm{O}(1/\alpha_x)$ near the interface, and very close to zero elsewhere, for $\alpha_x \gg 1$. A solution is shown in Fig. 7(D). Immediately we notice the similarity between our mean profile and that of Fulford and Blake (1986), as shown in Fig. 1.

Recalling that $u = (1/2)u_0 + \sum_{n=1}^{N} u_n$ where the u_n terms average to zero in time, for $\alpha_x \gg 1$ we have PCL flux

$$\int_0^h u \, \mathrm{d}y \sim \frac{-U_{\mathrm{int}} f_0 \theta_1 (1+\cos(\pi h))}{2\pi \sin(\pi h)}, \tag{64}$$

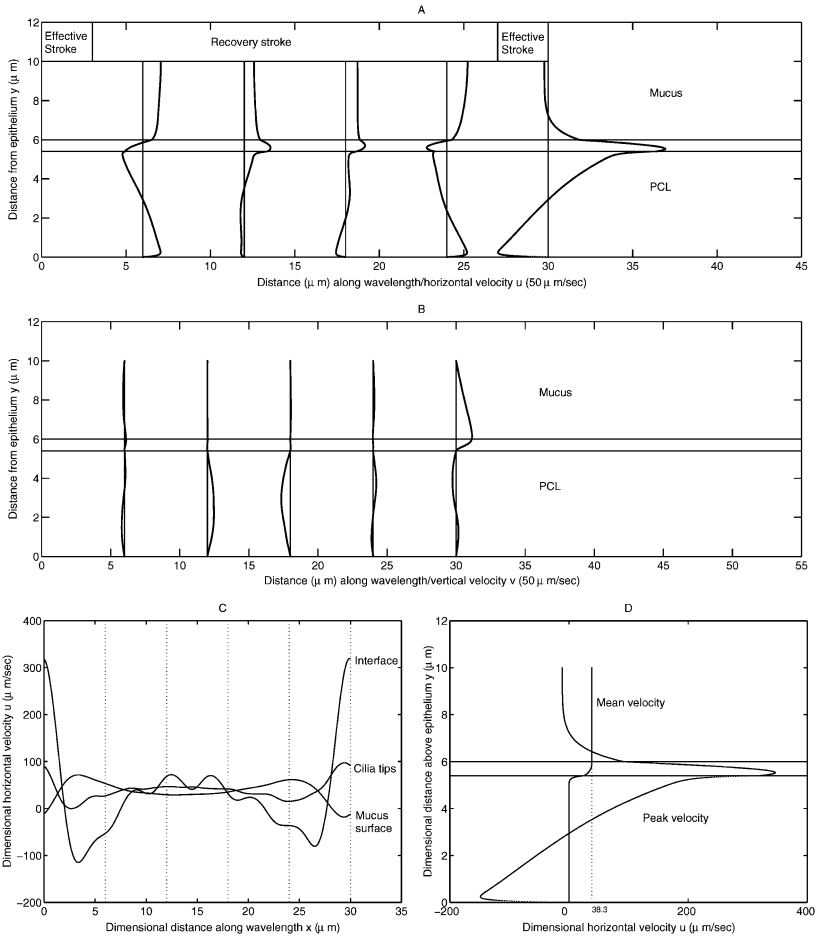

Fig. 7 Traction layer numerical results: (A) Horizontal velocity profiles at five points along the wavelength versus distance from epithelium. (B) Vertical velocity profiles at five points along the wavelength versus distance from epithelium. (C) Horizontal velocity at three different levels in the ASL, the PCL–mucus interface, the cilia tips $y = L$ and the mucus surface $y = H$, versus distance along the wavelength. (D) The mean and peak horizontal velocity versus height above epithelium. Dimensional parameter values: $L = 6\ \mu$m, $\lambda = 30\ \mu$m, $H = 10\ \mu$m, $h = 5.4\ \mu$m, $\nu = 5/6$, $\sigma = 60\ \text{rad}\,\text{s}^{-1}$, $\lambda_1 = 0.03\,$s. Viscosity ratios $\theta_1 = 6$, $\theta_2 = 8$. Sublayer resistance coefficients $\alpha_x = 90$, $\alpha_y = 75$.

and mucus flux

$$\int_h^H u\,\mathrm{d}y \sim \frac{-U_{\text{int}}\,f_0}{2\pi\,\sin(\pi h)}\left\{\frac{1}{2}(1-h)(2H-h-1)+\frac{1+\cos(\pi h)}{\pi^2}\right.$$
$$\left.-\frac{\sin(\pi h)}{\pi}(H-h)+\mathrm{O}\left(\frac{1}{\alpha_x}\right)\right\}. \tag{65}$$

Numerical values for the flux are given in Section 11.1

10. Numerical solution for $n \geqslant 1$

To solve the full ODE system we use the NAG library routine D02GAF. Details are given in Appendix B. The constants U_{int} and V_{int} are undetermined in the above. In order for the solution to be self-consistent, we require that $U_{\text{int}} = u - u_{\text{cilia}}$ and $V_{\text{int}} = v - v_{\text{cilia}}$ evaluated at $y = 0$. The condition is imposed at the apex of the effective stroke, $2\pi x + \sigma t = 0$. With the assumption that $v = 0$ at $y = h$, and the fact that by definition, $v_{\text{cilia}} = 0$ at $2\pi x + \sigma t = 0$, it follows that $V_{\text{int}} = 0$. It remains to determine U_{int}. To address this we use an iterative procedure as described next.

An initial estimate of U_{int} is made, together with upper and lower bounds. The steady velocity, as calculated in Section 9 is evaluated, then for $n = 1, \ldots, 15$ the above numerical system is solved. The steady and unsteady terms are summed to give the horizontal velocity u at the point $x = 0.0$, $y = h$, $t = 0.0$. We evaluate $u - u_{\text{cilia}}$, and adjust U_{int} using interval bisection. This is continued until convergence is achieved. For example, with our standard parameter set, we obtained $U_{\text{int}} = -0.026017$, $u - u_{\text{cilia}} = -0.026014$. The parameter U_{int} is hence responsible for coupling the Fourier modes, and causes the viscoelastic parameter λ_1 and the shear thinning ratio θ_2 to influence the mean transport, although they do not appear explicitly in Eq. (63).

11. Numerical results and discussion

In Fig. 7, we present graphs of the numerical results. The 'standard' parameter set which we use for reference is $L = 6\ \mu$m, $\lambda = 30\ \mu$m, $H = 10\ \mu$m, $h = 5.4\ \mu$m, $\sigma = 60$ rad s^{-1}, $\lambda_1 = 0.03$ s, $\theta_1 = 6$, $\theta_2 = 8$, $\alpha_x = 90$ and $\alpha_y = 75$. The resistance coefficients α_x and α_y are defined as in Eqs. (34) and (6), and determined from the parameters $d = 0.3\ \mu$m for the cilia spacing and $r = 0.1\ \mu$m for the cilium radius. Figure 7A shows the horizontal velocity profile at different stages in the beat cycle. Furthest to the right, the profile during the effective stroke is shown. There is a large forward flow of mucus close to the point of penetration, decaying to a value less than zero at the top of the mucous layer. In the PCL there is approximately equal forward and backward flow at the top and bottom of the layer, caused by the pressure gradient which maintains the interface at a constant height. It may be surprising that so close to the epithelium, the fluid velocity is relatively large. This is due to the effect of a large positive pressure gradient acting to maintain conservation of mass in the face of a large shearing motion in the active porous medium. It should be noted that the velocity is an average in the x_2 direction—into the paper—and that very close to the body of an individual cilium the fluid is likely to move with a very similar velocity to the cilium. During the recovery stroke, shown in the remaining four profiles, the mucus velocity is positive, a surprising finding since the cilia are beating backwards at this time. This is due to the effect of the pressure gradient in the mucus maintaining a constant forward flux. There is, nevertheless a backward flow of mucus in the traction layer at certain points during the recovery stroke. There is considerable elastic stretching of the mucous layer, which is made possible by the Maxwell element in the model.

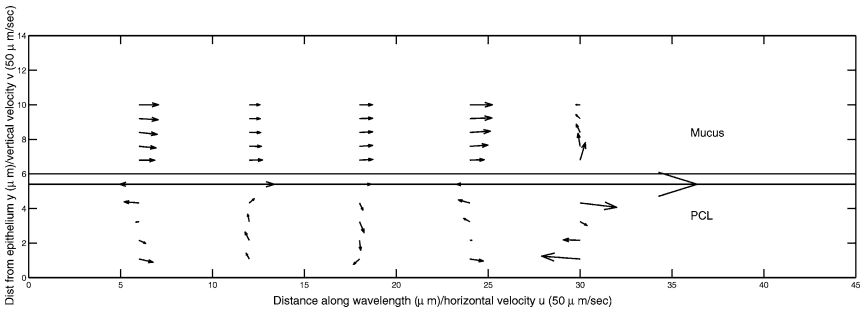

Fig. 8 Traction layer numerical results: quiver plot of the velocity field for the 'standard' parameter set $L = 6\ \mu$m, $\lambda = 30\ \mu$m, $H = 10\ \mu$m, $h = 5.4\ \mu$m, $\sigma = 60$ rad s^{-1}, $\lambda_1 = 0.03$ s. Viscosity ratios $\theta_1 = 6$, $\theta_2 = 8$. Sublayer resistance coefficients $\alpha_x = 90$, $\alpha_y = 75$, sublayer velocity scaling $\nu = 5/6$.

Figure 7B shows the corresponding vertical velocity profiles. By comparison, the vertical velocity is relatively small, likely due to the constraining effect of the flat surface and interface. Figure 7C shows the horizontal velocity at several different levels in the fluid, showing the predominantly positive mucus velocity at the surface and at $y = L$, and the large forward and backward oscillations at the level of the interface. Figure 7D compares the peak velocity at the time of penetration with the mean flow of mucus. The mean profile is very similar to the Fulford and Blake (1986) profile, depicted in Fig. 1A.

We also present a 'quiver plot' of the velocity field, in Fig. 8. This graph shows more clearly that the mucus above $y = L$ flows nearly uniformly and steadily throughout most of the beat cycle, except for the time of penetration. In addition, this plot shows interesting circulation patterns in the PCL caused by the interaction of the ciliary beat and the pressure gradients. These circulation patterns may assist in the transfer of particles, for instance pathogens, or tracer particles in the experiments of Matsui et al. (1998), from the PCL to the mucous layer for efficient removal.

11.1. PCL and mucus flux results

For the standard parameter set, $U_{\text{int}} = -0.026017$. From Eq. (64), the nondimensional PCL flux is 7.87×10^{-4}, corresponding to a dimensional value of 1.70 μm^2 s^{-1}. This compares with a mucus flux of 8.07×10^{-2}, corresponding to a dimensional value of 174 μm^2 s^{-1}. The flux of mucus is over 100 times greater than that of PCL, due to the viscous resistance of the cilia.

11.2. Mean mucus transport

Our simulation using the standard parameter set predicts a mean mucus velocity of 38.3 μm s^{-1}. Salathe et al. (1997) report a range of values of between 67 and

Table 1 Mucus transport values for various parameter sets.

Parameters	Mean mucus velocity[a] (μ m s^{-1})
Standard	38.3
σ =36 rad s^{-1}	22.3 ($\downarrow$ 41.8)
$\lambda_1 = 0.00$ s	60.9 ($\uparrow$ 59.0)
$\lambda_1 = 0.01$ s	47.2 ($\uparrow$ 23.2)
$\lambda_1 = 0.04$ s	44.9 ($\uparrow$ 17.2)
$H = 6.5$ μm	59.2 ($\uparrow$ 54.6)
$H = 12$ μm	36.4 ($\downarrow$ 4.96)

Note. The standard parameter set is $L = 6$ μ m, $\lambda = 30$ μ m, $H = 10$ μ m, $h = 5.4$ μ m, $\nu = 5/6$, $\sigma = 60$ rad s^{-1}, $\lambda_1 = 0.03$ s, $\theta_1 = 6$, $\theta_2 = 8$, $\alpha_x = 90$ and $\alpha_y = 75$.
[a]The values in parentheses are the percentage values.

333 μm s^{-1}, the authors believing that the first figure, based on less invasive meansuring techniques, is likely to be more accurate. Reviewing the results of similar studies, ICRP (1994) reported a wide range of values depending upon disease, ambient conditions and other factors. For healthy subjects, values of 70 and 92 μm s^{-1} for tracheal transport, and 40 μm s^{-1} for bronchial transport were reported. Finally, the hTBE cultures studied by Matsui et al. (1998) showed a mean transport of 39.2 μm s^{-1}, very close to our predicted value.

To summarise the effect on mucus transport of different parameter sets, we present Table 1. Decreasing the rate of ciliary beating within the experimentally observed range (Salathe et al., 1997) by 40% to 36 rad s^{-1} results in an approximately proportionate reduction in transport. Increasing the mucus 'stiffness' by reducing the relaxation time to 0.01 s significantly increases mucus transport by 23%, and surprisingly increasing the relaxation time to 0.04 s also results in an increase in transport of 17%. Perhaps most surprisingly, setting $\lambda_1 = 0$, equivalent to Newtonian 'mucus', results in greatly enhanced transport. The role of mucus viscoelasticity is hence more complex than can be elucidated by our model. It is possible that there are molecular level interactions between polymer chains and the cilia tips. It is also possible that viscoelasticity serves some other purpose, for instance in the trapping of particles or in enhancing transport over non-ciliated regions. This should be a subject for future study.

Deeper mucus ($H = 12$ μm) leads to only slightly slower mucus transport, provided that such parameters as the ciliary beat frequency and the mucus viscosity remain the same. Due to the thickened layer, the cilia are actually propelling a considerably larger volume of mucus. This suggests that if a thicker (deeper) mucus is observed in patients with impaired mucus transport, it may not be the thickness *per se* that causes the impairment, but rather it may simply be a symptom of reduced transport. Conversely, this provides insight into how the body adapts to a thickening mucous layer moving from the bronchioles to the trachea—the cilia do not need to beat significantly faster to transport a greater volume of mucus. A greatly depleted, but still continuous, mucous layer represented by $H = 6.5$ μm shows transport increased significantly by 54.6%.

11.3. Understanding the effects of different physical parameters on transport

Examining Eq. (63) we see that there are various ways in which mucus transport can be altered. The mucus velocity u^{M2} is proportional to the interaction velocity $-U_{\text{int}}$ and the first term in braces is proportional to the traction layer viscosity θ_1. Simply altering the value of the beat frequency σ, all else being equal, will have a proportionate effect on mucus transport. In addition, all of the parameters interact in a nonlinear way to affect $-U_{\text{int}}$, which we explore next. Furthermore, the dimensional value of u^{M2} is proportional to σ.

For brevity we write the fluid velocity at the apex of the effective stroke as $u_{\text{pen}} = u(2\pi x + \sigma t = 0, y = h)$. Since $-U_{\text{int}} = u_{\text{cilia}} - u_{\text{pen}}$ it is clear that reducing the value of u_{pen} will increase $-U_{\text{int}}$ and hence the mean mucus velocity. In general, physical effects that resist the sharp forward flow of mucus in response to penetration will tend to decrease u_{pen} and hence increase transport. The effect of a positive instantaneous pressure gradient $\mathrm{d}p/\mathrm{d}x$ is to act as a resistance force to the forward flow of liquid, as can be seen from Eq. (30). At the point of penetration, this results in a reduction in u_{pen} and hence an increase in $-U_{\text{int}}$ and mucus transport.

Hence, the results in Table 1 can be understood physically. Reducing the relaxation time of the mucus to 0.01 s effectively reduces how readily the mucus will deform elastically in response to penetration. The value of u_{pen} is hence smaller and so $-U_{\text{int}}$ is increased, and hence the mean transport. Increasing the relaxation time to 0.04 s increases the elasticity of the mucus, and at the same time increases the positive pressure gradient in the upper part of the PCL. This has the overall effect of reducing u_{pen} and hence increasing the mucus transport. Decreasing the depth of the mucous layer greatly increases the effect of the mucus free surface and hence increases the pressure gradient by about 50%, decreasing u_{pen} and hence increasing transport.

11.4. Shear-thinning ratio

We were not able to determine parameters for the shear-thinning ratio, so we have produced results for a spectrum of values of θ_1 and θ_2 corresponding to a fixed free mucus viscosity of $\mu^{M2} = \theta_1\theta_2 = 48$. The effect on mean mucus transport is shown in Fig. 9. For values of θ_1 close to 3, a sharp spike occurs (not shown). This is due to the fact that the pressure gradient in the PCL enforcing $v(y = h) = 0$ becomes large and negative. In reality, the interface would simply deform, and our model assumptions would break down. Since the interface does not appear to move significantly in the micrographs of Sanderson and Sleigh (1981), it is likely that the viscosity of the traction layer does not approach this value. For the standard parameter set, the jump in normal stress at the mucus–PCL interface is no larger than 100 $\mathrm{N\,m^{-2}}$. For $\theta_1 = 2.995$, the jump in normal stress reaches 1000 $\mathrm{N\,m^{-2}}$. To balance this, the surface tension force must be 10 times larger, which corresponds to the curvature of the interface being 10 times larger. Again estimating the surface tension to be 0.08 $\mathrm{N\,m^{-1}}$, the curvature must increase from 1250 $\mathrm{m^{-1}}$ to 12, 500 $\mathrm{m^{-1}}$. If we make the simple assumption that the interface has the form $\eta = \eta_0 + \varepsilon\,\cos(kx + \sigma t)$, for some small perturbation ε, the curvature can

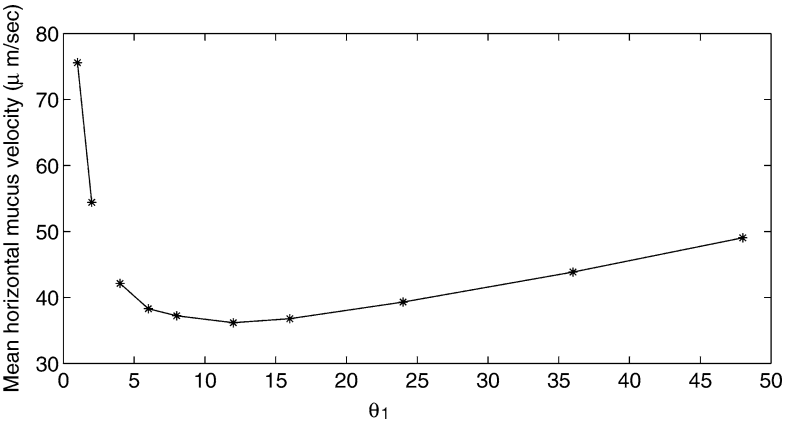

Fig. 9 Mean mucus transport against traction layer viscosity θ_1 for fixed mucus viscosity $\theta_1\theta_2 = 48$. Sublayer resistance coefficients $\alpha_x = 90$, $\alpha_y = 75$, sublayer velocity scaling $\nu = 5/6$. Model assumptions were not justified for $\theta_1 \sim 3$.

be approximated by $|\eta_{xx}| = \varepsilon k^2$. If the wavenumber $k = 2\pi/3.0 \times 10^{-5}$ m^{-1}, then ε must increase from 2.8×10^{-2} to 0.28 μm, a significant disturbance on the scale of the muco-ciliary system.

Even ignoring this point, the relationship between transport and θ_1 is still nonlinear, with transport being greatest at $\theta_1 = 1$, and also being greater at $\theta_1 = 48$ than at $\theta_1 = 6$. For $\theta_1 = 1$, the PCL has a significant effect on the traction layer, through the boundary condition (50). Hence, the positive pressure gradient in the PCL, which resists the flow of fluid has a significant effect, reducing u_{pen}. Conversely, for $\theta_1 = 48$, the upper mucus layer now has a significant effect on the traction layer, through the boundary condition 53.

11.5. The relative importance of pressure gradients in the mucus and PCL

In addition to the above we have investigated similar models (not shown), with no pressure in the mucous layer, and with no pressure anywhere in the fluid. With no pressure at all we found only a very small mean mucus velocity—1.63 μm s^{-1} for the standard parameter set. The model with no pressure in the mucous layer only predicted very similar mucus transport to the model presented here. This suggests that it is the action of pressure gradients in the PCL, rather than the mucous layer that are essential to ensuring positive transport of mucus. This calls into question the earlier suggestion of Sleigh et al. (1988) that there is no significant interface tension between the PCL and mucus.

11.6. Modelling diseased states

Our model is more suitable for comparison with diseases such as chronic obstructive pulmonary disease (COPD) or asthma, in which the distinct PCL and mucous layers and interface are more clearly preserved, than diseases such as cystic

Table 2 Table of mucus transport values for various possible 'diseased' states.

Parameters	Mean mucus velocity[a] (μm s^{-1})
Standard	38.3
Very slow ciliary beating $\sigma = 10$ rad s^{-1}	7.33 ($\downarrow$ 80.9)
Very viscous mucus $\theta_1 = 30, \theta_2 = 30$	56.8 ($\uparrow$ 48.3)
'Watery' mucus $\lambda_1 = 0, \theta_1 = 1, \theta_2 = 1$	58.8 ($\uparrow$ 53.5)
Elastic, 'watery' mucus $\lambda_1 = 0.03$ s, $\theta_1 = 1, \theta_2 = 1$	58.6 ($\uparrow$ 53.0)
Deeper, less viscous mucus $H = 40$ μm,$\theta_1 = 8, \theta_2 = 1$	26.6 ($\downarrow$ 30.5)
Double viscosity $\theta_1 = 12, \theta_2 = 8$	39.1 ($\uparrow$ 2.08)

[a]The values in parentheses are the percentage values.

fibrosis, in which mucins may be found in the PCL, and in which the PCL may be significantly depleted. Detailed comparisons of these conditions may be found in Rogers (2004) and Boucher et al. (2000). In Table 2 we present some results providing a tentative simulation of various 'diseased' states of the muco-ciliary system. As one might expect, our model predicts that if the ciliary beat frequency is greatly reduced from 60 rad s^{-1} by 83% to 10 rad s^{-1}, mucus transport is reduced almost proportionately. Hence, one likely cause of impaired clearance is reduced ciliary beating. Surprisingly, altered rheological parameters such as much more viscous ($\theta_1 = \theta_2 = 30$), or much more 'watery' mucus ($\lambda_1 = 0, \theta_1 = \theta_2 = 1$), or more elastic or Newtonian mucus ($\lambda_1 = 0.04, \lambda_1 = 0$), do not seem to significantly impair mucus clearance when compared with our initial parameter set. It is possible, however, that more viscous or less elastic mucus may have a more subtle effect by impairing ciliary beating.

The results appear to show that mucus is important to transport by producing an interface which supports pressure gradients in the PCL. The pressure gradients need have no mean effect, but they nevertheless allow the cilia to interact with the upper layer efficiently. The viscoelastic interaction of mucus and cilia itself appears not to be the important mechanism. Nevertheless, it is also possible that mucus elasticity is important in the interaction of the cilium tip and the mucous layer. Detailed observation and mathematical modelling of this interaction will provide further insight.

To simulate the effect of excessive fluid secretion, we chose the parameters $H = 40$ μm, $\theta_1 = 8$, $\theta_2 = 1$, representing a deep, less viscous mucous layer. The effect was to reduce velocity to 26.6 μm s^{-1}, which although significantly less than the standard parameters, was not the virtual cessation of transport one might expect. However, as discussed by Blake (1973), a very deep mucous layer will be subject to significant gravitational force, which was not included in our model. In addition, deeper mucus may result in 'plugging' of airways, and disruption of the normal surface and interface properties. It should also be noted that for a deep mucus layer or a very narrow airway, curvature in the x_2 direction will no longer be negligible (Rogers, 2004), and may lead to important pressure gradients caused by surface tension.

In summary, nothing short of a cessation of normal ciliary beating appears sufficient to interupt muco-ciliary functioning in our model. However, the fact that transport is so impaired by the lack of a pressure gradient in the PCL caused by

interface tension suggests strongly that mucus–PCL interaction is important for maintaining efficient transport. For instance, excessive surfactant may, by lowering interface tension, impair the system. Our 'interface' is an idealisation of the real system, which is known to deform in order to allow ciliary penetration (Puchelle et al., 1998). Future modelling work should investigate the role of this region further.

12. Comparision with experimental studies

Our simulations of disease states, which suggest that low mucus viscosity and elasticity do not harm, and indeed benefit transport, and that ciliary beat frequency is the most important determinant of normal functioning, show some interesting parallels with experimental studies, though these must be qualified by the fact that we have currently only considered an impermeable epithelium.

A study of patients with pseudohypoaldosteronism (PHA) (Kerem et al., 1999) showed that no liquid is absorbed from the ASL by the epithelium, and consequent greatly enhanced mucus transport. Our results showing enhanced transport for 'watery mucus' support the hypothesis that increased water content of ASL, even beyond the normal level, is beneficial to transport. Shibuya et al. (2003) used a bovine trachea model to test the effect of both osmolality and liquid depletion on viscosity and transport. Adding sodium caused a highly significant increase in transport, whereas iso-osmolal removal of liquid resulted in approximately a doubling of 'viscoelasticity,' and a nonsignificant increase in transport. This is qualitatively similar to our results predicting a very modest increase in transport of 2% for doubled mucus viscosity.

Mucolytic drugs, designed to reduce mucus viscosity, have been studied in an attempt to improve muco-ciliary transport and hence alleviate muco-ciliary disfunction. However (Salathe et al., 1996; Rogers, 2005), mucolytics have tended to be ineffective for improving muco-ciliary transport *in vivo*. Symptoms of chronic bronchitis and chronic obstructive pulmonary disease have been slightly improved by the use of oral mucolytics (Poole and Black, 2001), but this modest benefit may be due to mechanisms other than improving muco-ciliary transport, such as antioxidant properties (Ekberg-Jansson et al., 2001), anti-inflammatory properties (Gibbs et al., 1999) or through increasing the water content of the ASL (Rochat et al., 2004). Our results showing that mucus viscosity does not have any clear effect on transport are consistent with these findings.

Finally, β_2-adrenergic agents such as salbutamol and salmeterol have been shown to enhance ciliary beat frequency (Devalia et al., 1992) and salmeterol has been shown to slightly enhance muco-ciliary clearance in patients with asthma (Hasani et al., 2003). Conversely, the β-blocking drug propanolol depresses muco-ciliary clearance significantly (Pavia et al., 1986), consistent with our findings.

13. Conclusions and future work

We presented a model of mucus transport which represented the propulsive and resistive effects of the cilia by volume forces, and represented mucus as a linearised Maxwell fluid. Our model incorporated metachronism, the periodicity

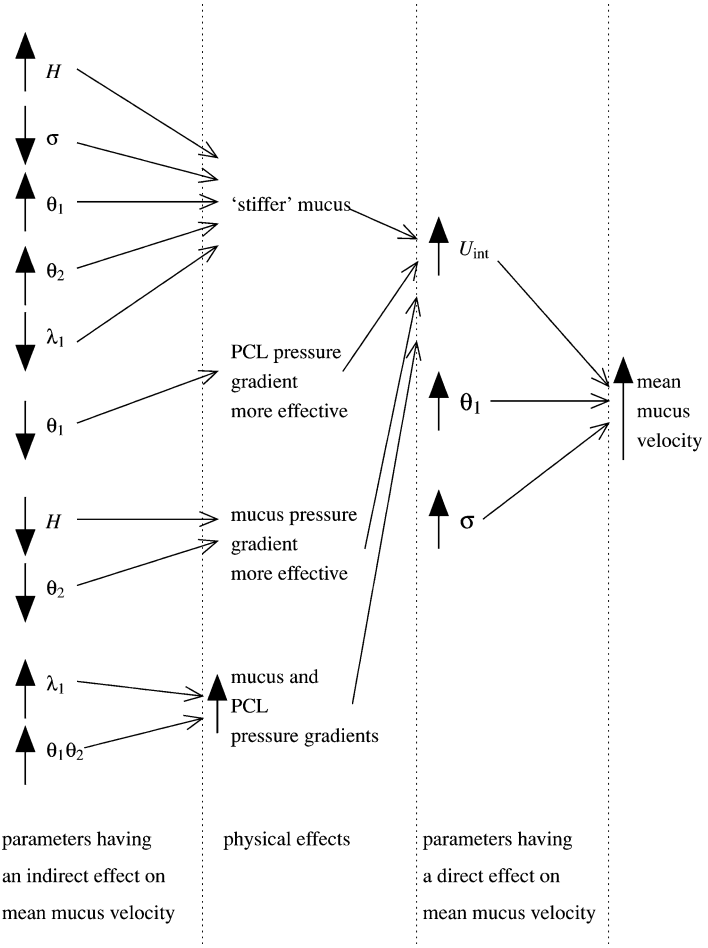

Fig. 10 Schematic diagram of the influence of various physical parameters on mean mucus velocity. Working from the right, increases in the interaction velocity U_{int}, the traction layer viscosity θ_1 and the beat frequency σ all directly increase mean mucus velocity, as shown in Eq. (63). The interaction velocity U_{int} may be increased by 'stiffer' mucus, by increasing the PCL and mucus pressure gradients, and by increasing the effect of the PCL and mucus pressure gradients. These effects are in turn caused by various changes to the model parameters, for instance increases in the relaxation time λ_1 and the mucous layer viscosity $\theta_1\theta_2$ both cause an increase in mucus and PCL pressure gradients. Note that most parameters do not have a simple effect; for instance increasing the depth of the ASL by increasing H leads to 'stiffer' mucus, increasing U_{int}, hence tending to increase mean mucus velocity. However, increasing H will also render the pressure gradient in the mucous layer less effective, which tends to have the opposite effect. The overall effect of increasing H from 10 to 40 μm is shown in Table 2, a 30.5% decrease.

of the ciliary beat, resistance of the cilia sublayer, spatial variations in the propulsive force, a linear model of viscoelasticity of the mucous layer and surface and interface tension, giving more insight regarding the temporal and spatial detail of the flow than previously published models. By exploiting the periodicity of the beat cycle, we converted the fluid flow equations into a system of coupled

ordinary differential equations. We then calculated numerical solutions for various parameter sets, assuming that surface and interface movement was negligible.

Subject to the assumption of no-flux through the epithelium and consistent with the hypotonic defensin hypothesis, the time-averaged horizontal profile is qualitatively very similar to the results of Fulford and Blake (1986), and the earlier work of Blake and Winet (1980) and unlike that predicted by Matsui et al. (1998). This demonstrates that a detailed model consistent with the hypotonic defensin hypothesis produces PCL flux inconsistent with the conclusions of Matsui et al. (1998), even with the novel incorporation of mucus viscoelasticity, surface tension and pressure gradients. Clearly, it will be of considerable interest to determine whether models incorporating transepithelial fluxes, and thus consistent with the isotonic volume hypothesis, produce significantly different results. In addition, we observed large oscillations in the PCL relative to the net mucus transport, and circulation patterns in the PCL that may assist in the mixing and removal of tracer particles or contaminants. We are currently developing a model of tracer dispersion in the ASL, which will provide insight into whether our predicted fluid flow profiles are consistent with experiment (Smith et al., 2006).

Our model predicted physiologically reasonable values for mucus transport, from physiologically justified parameter sets. Our results predicted several interesting properties of the muco-ciliary system. The dependence of transport on the choice of physical parameters was nonlinear. It emerged that transport was only significantly disrupted by a reduction in σ. The system was remarkably robust to changes in other parameters, although this is notwithstanding the assumption that the PCL–mucus interface and mucus surface remain flat. It might be expected that the muco-ciliary system has evolved to function efficiently even when subjected to various changes in physical properties. Pressure gradients with zero mean, brought about by the interface and surface tension were crucial to ensuring efficient interaction between the mucus and cilia. Consistent with recent experimental findings, ciliary beat frequency was a crucial determinant of efficient transport, and 'watery' mucus was transported more efficiently than normal mucus.

There are a number of ways the model could be developed. The cilium–mucus interaction is difficult to represent in a simple way. There are many cilium bodies penetrating the mucus, at different angles, in the presence of surface forces, with possible molecular level interactions taking place. The role of surfactant in allowing cilia tips to deform and penetrate the mucus may be very interesting to investigate, and it will be instructive to test what happens when our assumptions regarding the flat surface and interface are relaxed. To model further the way in which different physical parameters interact, it would be necessary to model the internal mechanics and energy consumption of the cilia, as has been done by Gueron and Liron (1992), so that for instance we could test whether increasing viscosity would affect beat frequency. It is also known that the presence of mucus provides a stimulus for ciliary beating (Sleigh et al., 1988)—investigating possible mechanisms for this coupling may be developed. It might also be useful to model movement of the surface and interface, and the surface tension forces this would produce. Integration of more detailed models of mucus rheology, such as that of Quemada (1984) with the fluid flow equations may provide still more insight, as would considering possible non-Newtonian effects in the PCL (Boucher, 2003).

Finally, our model of the behaviour of the 'active porous medium' is only an approximation of the beating cilia. In particular, there is a gap between the tips of the cilia and the mucus interface throughout the recovery stroke, which was not a feature of our model. In Smith (2006), we develop a singularity model of the field of cilia in order to model the flow in the PCL more accurately.

Acknowledgements

D. J. Smith thanks EPSRC for financial support. The authors also thank faculty and students at the Cystic Fibrosis/Pulmonary Research and Treatment Center and the Department of Applied Mathematics, University of North Carolina, Chapel Hill, for valuable discussions regarding this work, and for insights regarding how this model may be developed further.

Appendix

A. Fourier coefficients

A.1. Force coefficients f_n, g_n

$f_0 = 0.2$, $f_1 = 0.19351$, $f_2 = 0.17503$, $f_3 = 0.14737$
$f_4 = 0.11456$, $f_5 = 0.08106$, $f_6 = 0.05091$, $f_7 = 0.02707$
$f_8 = 0.01094$, $f_9 = 0.00239$, $f_{10} = 0.0$, $f_{11} = 0.00160$
$f_{12} = 0.00486$, $f_{13} = 0.00785$, $f_{14} = 0.00935$, $f_{15} = 0.00901$

$g_0 = 0.0$, $g_1 = -0.04905$, $g_2 = -0.08745$, $g_3 = -0.10731$
$g_4 = -0.10565$, $g_5 = -0.08488$, $g_6 = -0.05195$, $g_7 = -0.01611$
$g_8 = 0.01363$, $g_9 = 0.03101$, $g_{10} = 0.03396$, $g_{11} = 0.02469$
$g_{12} = 0.00855$, $g_{13} = -0.00785$, $g_{14} = -0.01900$, $g_{15} = -0.02183$

A.2. Active porous medium motion coefficients c_n, d_n

$c_0 = 0$, $c_1 = 0.46775$, $c_2 = 0.37843$, $c_3 = 0.25228$
$c_4 = 0.1169$, $c_n = 0.0$ $(n \geq 5)$
$d_0 = 0$, $d_1 = 0.09217$, $d_2 = -0.19211$, $d_3 = -0.23553$
$d_4 = -0.23148$, $d_5 = -0.18536$, $d_6 = -0.11252$, $d_7 = -0.03354$
$d_n = 0$ (n ≥ 8).

B. Numerical solution

B.1. Transforming the domain

In order to solve the system numerically it must be rewritten in the form

$$Y_i' = F_i(X, Y_1, \ldots, Y_{30})$$

for $i = 1, \ldots, 30$, and solved on a domain $0 < X < 1$. We make the following transformations:

In the PCL $y = hX$, $\mathrm{d}/\mathrm{d}y = (1/h)\mathrm{d}/\mathrm{d}X$, $y = 0, \ldots, h$, $X = 0, \ldots, 1$. In the traction layer $y = 1 - (1-h)X$, $\mathrm{d}/\mathrm{d}y = -1/(1-h)\mathrm{d}/\mathrm{d}X$, $y = h, \ldots, 1$, $X = 1, \ldots, 0$. In the force-free mucous layer $y = 1 + (H-1)X$, $\mathrm{d}/\mathrm{d}y = 1/(H-1)\mathrm{d}/\mathrm{d}X$, $y = 1, \ldots, H$, $X = 0, \ldots, 1$.

B.2. Variables of the ODE system

We now define the variables $Y_1, \ldots, Y_{30}$ in order to write the boundary and matching conditions in the form $Y_i = 0$ at $X = 0$ or $X = 1$.

$$
\begin{aligned}
Y_1 &= \check{u}^{\mathrm{r}}_{\mathrm{P}}, & Y_{11} &= \check{u}^{\mathrm{r}}_{\mathrm{P}} - \check{u}^{\mathrm{r}}_{\mathrm{M1}},\\
Y_2 &= \check{u}^{\mathrm{i}}_{\mathrm{P}}, & Y_{12} &= \check{u}^{\mathrm{i}}_{\mathrm{P}} - \check{u}^{\mathrm{i}}_{\mathrm{M1}},\\
Y_3 &= \check{v}^{\mathrm{r}}_{\mathrm{P}}, & Y_{13} &= \check{v}^{\mathrm{r}}_{\mathrm{P}} - \check{v}^{\mathrm{r}}_{\mathrm{M1}},\\
Y_4 &= \check{v}^{\mathrm{i}}_{\mathrm{P}}, & Y_{14} &= \check{v}^{\mathrm{i}}_{\mathrm{P}} - \check{v}^{\mathrm{i}}_{\mathrm{M1}},\\
Y_5 &= -2\pi n\check{u}^{\mathrm{i}}_{\mathrm{P}} + \check{v}^{\mathrm{r}'}_{\mathrm{P}}/h, & Y_{15} &= -2\pi n\check{u}^{\mathrm{i}}_{\mathrm{M1}} - \check{v}^{\mathrm{r}'}_{\mathrm{M1}}/(1-h),
\end{aligned}
$$

$$
\begin{aligned}
Y_6 &= 2\pi n\check{u}^{\mathrm{r}}_{\mathrm{P}} + \check{v}^{\mathrm{i}'}_{\mathrm{P}}/h,\\
Y_7 &= \phi\check{u}^{\mathrm{r}'}_{\mathrm{P}}/h - \psi\check{u}^{\mathrm{i}'}_{\mathrm{P}}/h - 2\pi n\varepsilon^2\big(\phi\check{v}^{\mathrm{i}}_{\mathrm{P}} + \psi\check{v}^{\mathrm{i}'}_{\mathrm{P}} - \theta_1\check{v}^{\mathrm{i}}_{\mathrm{M1}}\big) + \theta_1\check{u}^{\mathrm{r}'}_{\mathrm{M1}}/(1-h),\\
Y_8 &= \phi\check{u}^{\mathrm{i}'}_{\mathrm{P}}/h + \psi\check{u}^{\mathrm{r}'}_{\mathrm{P}}/h - 2\pi n\varepsilon^2\big(\psi\check{v}^{\mathrm{i}}_{\mathrm{P}} - \phi\check{v}^{\mathrm{i}'}_{\mathrm{P}} + \theta_1\check{v}^{\mathrm{r}}_{\mathrm{M1}}\big) + \theta_1\check{u}^{\mathrm{i}'}_{\mathrm{M1}}/(1-h),\\
Y_9 &= \check{p}^{\mathrm{r}}_{\mathrm{P}},\\
Y_{10} &= \check{p}^{\mathrm{i}}_{\mathrm{P}},\\
Y_{16} &= 2\pi n\check{u}^{\mathrm{r}}_{\mathrm{M1}} - \check{v}^{\mathrm{i}'}_{\mathrm{M1}}/(1-h),\\
Y_{17} &= -\check{u}^{\mathrm{r}'}_{\mathrm{M1}}/(1-h) - 2\pi n\varepsilon^2\check{v}^{\mathrm{i}}_{\mathrm{M1}} - \theta_2\check{u}^{\mathrm{r}'}_{\mathrm{M2}}/(H-1) + 2\pi n\theta_2\varepsilon^2\check{v}^{\mathrm{i}}_{\mathrm{M2}},\\
Y_{18} &= -\check{u}^{\mathrm{i}'}_{\mathrm{M1}}/(1-h) + 2\pi n\varepsilon^2\check{v}^{\mathrm{r}}_{\mathrm{M1}} - \theta_2\check{u}^{\mathrm{i}'}_{\mathrm{M2}}/(H-1) - 2\pi n\theta_2\varepsilon^2\check{v}^{\mathrm{r}}_{\mathrm{M2}},\\
Y_{19} &= -\check{p}^{\mathrm{r}}_{\mathrm{M1}} - 2\varepsilon^2\check{v}^{\mathrm{r}'}_{\mathrm{M1}}/(1-h) + \theta_2\check{p}^{\mathrm{r}}_{\mathrm{M2}} - 2\theta_2\varepsilon^2\check{v}^{\mathrm{r}'}_{\mathrm{M2}}/(H-1),\\
Y_{20} &= -\check{p}^{\mathrm{i}}_{\mathrm{M1}} - 2\varepsilon^2\check{v}^{\mathrm{i}'}_{\mathrm{M1}}/(1-h) + \theta_2\check{p}^{\mathrm{i}}_{\mathrm{M2}} - 2\theta_2\varepsilon^2\check{v}^{\mathrm{i}'}_{\mathrm{M2}}/(H-1),
\end{aligned}
$$

$$
\begin{aligned}
Y_{21} &= \check{u}^{\mathrm{r}}_{\mathrm{M1}} - \check{u}^{\mathrm{r}}_{\mathrm{M2}}, & Y_{26} &= 2\pi n\check{u}^{\mathrm{r}}_{\mathrm{M2}} + \check{v}^{\mathrm{i}'}_{\mathrm{M2}}/(H-1),\\
Y_{22} &= \check{u}^{\mathrm{i}}_{\mathrm{M1}} - \check{u}^{\mathrm{i}}_{\mathrm{M2}}, & Y_{27} &= \check{u}^{\mathrm{r}'}_{\mathrm{M2}}/(H-1) - 2\pi n\varepsilon^2\check{v}^{\mathrm{i}}_{\mathrm{M2}},\\
Y_{23} &= \check{v}^{\mathrm{r}}_{\mathrm{M1}} - \check{v}^{\mathrm{r}}_{\mathrm{M2}}, & Y_{28} &= \check{u}^{\mathrm{i}'}_{\mathrm{M2}}/(H-1) + 2\pi n\varepsilon^2\check{v}^{\mathrm{r}}_{\mathrm{M2}},\\
Y_{24} &= \check{v}^{\mathrm{i}}_{\mathrm{M1}} - \check{v}^{\mathrm{i}}_{\mathrm{M2}}, & Y_{29} &= \check{p}^{\mathrm{r}}_{\mathrm{M2}},\\
Y_{25} &= -2\pi n\check{u}^{\mathrm{i}}_{\mathrm{M2}} + \check{v}^{\mathrm{r}'}_{\mathrm{M2}}/(H-1), & Y_{30} &= \check{p}^{\mathrm{i}}_{\mathrm{M2}}.
\end{aligned}
$$

The boundary conditions take the form $Y_i = 0$ on $X = 0$ for $i = 1, \ldots, 6$, $17, \ldots, 26$, and $Y_i = 0$ on $X = 1$ for $i = 3, 4$, $i = 7, 8$, $i = 11, \ldots, 16$, $i = 23, 24, 27, 28$. There are no boundary conditions for the pressure Y_9, Y_{10}, Y_{29} and Y_{30}, but two boundary conditions for Y_3, Y_4, Y_{23} and Y_{24}, so that there are 30 boundary conditions for 30 variables. The algorithm D02GAF starts with an initial approximation calculated from the boundary conditions and estimates of the solution at boundary points for which there is no boundary condition. This is then improved

using a finite difference technique with deferred correction. Writing the system of 18 ODEs in terms of these variables we have

$$h(\phi^2+\psi^2)\big(-2\pi nY_{10}+\big(\beta_x^2+\chi^2\big)Y_1-\nu Xhc_n\alpha_x^2-2\pi n\varepsilon^2Y_6\big)$$
$$=\phi Y_7'+\psi Y_8'+\theta_1\phi Y_{17}'+\theta_1\theta_2\psi Y_{27}'+\theta_1\psi Y_{18}'+\theta_1\theta_2\psi Y_{28}'$$

$$h(\phi^2+\psi^2)(2\pi nY_9+\big(\beta_x^2+\chi^2\big)Y_2+2\pi n\varepsilon^2Y_5)$$
$$=\phi Y_8'-\psi Y_7'-\theta_1\psi Y_{17}'-\theta_1\theta_2\phi Y_{27}'+\theta_1\phi Y_{18}'+\theta_1\theta_2\phi Y_{28}'$$

$$(\phi^2+\psi^2)(Y_9'+\big(\chi^2+\beta_y^2\big)\varepsilon^2hY_3)$$
$$=2\pi nh\varepsilon^2[\phi Y_8-\psi Y_7-\theta_1\psi Y_{17}-\theta_1\theta_2\psi Y_{27}+\theta_1\phi Y_{18}+\theta_1\theta_2\phi Y_{28}]$$

$$(\phi^2+\psi^2)(Y_{10}'+\big(\chi^2+\beta_y^2\big)\varepsilon^2hY_4)$$
$$=-2\pi nh\varepsilon^2[\phi Y_7+\psi Y_8+\theta_1\phi Y_{17}+\theta_1\theta_2\phi Y_{27}+\theta_1\psi Y_{18}+\theta_1\theta_2\psi Y_{28}]$$
$$-\nu h^2d_n\alpha_y^2\varepsilon(\phi^2+\psi^2)X,$$

$$Y_5'=0,$$
$$Y_6'=0,$$

$$-2\pi n[-Y_{20}+2\varepsilon^2Y_{16}+\theta_2Y_{30}]-2\chi^2\theta_2(Y_1-Y_{11}-Y_{21})+4\pi n\theta_2\varepsilon^2Y_{26}$$
$$=-4\chi^2(Y_1-Y_{11})-(Y_{17}'+\theta_2Y_{27}')/(1-h)+2\pi n\varepsilon^2Y_{16}$$
$$-\phi f_n\alpha_x^2U_{\text{int}}\sin(\pi(1-(1-h)X))/\sin(\pi h),$$

$$2\pi n[-Y_{19}+2\varepsilon^2Y_{15}+\theta_2Y_{29}]-2\chi^2\theta_2(Y_2-Y_{12}-Y_{22})-4\pi n\theta_2\varepsilon^2Y_{25},$$
$$=-4\chi^2(Y_2-Y_{12})-(Y_{18}'+\theta_2Y_{28}')/(1-h)-2\pi n\varepsilon^2Y_{15}$$
$$-\psi f_n\alpha_x^2U_{\text{int}}\sin(\pi(1-(1-h)X))/\sin(\pi h),$$

$$Y_{19}'-4\pi n\varepsilon^2(Y_2'-Y_{12}')-\theta_2Y_{29}'-4\pi n\varepsilon^2\theta_2(Y_2-Y_{12}-Y_{22})=(1-h)$$
$$(-2\chi^2\varepsilon^2(Y_3-Y_{13})+2\pi n(Y_{18}+\theta_2Y_{28})$$
$$-\varepsilon\psi g_n\alpha_y^2V_{\text{int}}\sin(\pi(1-(1-h)X))/\sin(\pi h)).$$

$$Y_{20}'+4\pi n\varepsilon^2(Y_1'-Y_{11}')-\theta_2Y_{30}'+4\pi n\varepsilon^2\theta_2(Y_1-Y_{11}-Y_{21})=(1-h)$$
$$(-2\chi^2\varepsilon^2(Y_4-Y_{14})-2\pi n(Y_{17}+\theta_2Y_{27})$$
$$+\varepsilon\phi g_n\alpha_y^2V_{\text{int}}\sin(\pi(1-(1-h)X))/\sin(\pi h)).$$

$$Y_{15}'=0,$$
$$Y_{16}'=0,$$
$$Y_{27}'=(H-1)(2\chi^2(Y_1-Y_{11}-Y_{21})-2\pi n\varepsilon^2Y_{26}-2\pi nY_{30}),$$
$$Y_{28}'=(H-1)(2\chi^2(Y_2-Y_{12}-Y_{22})+2\pi n\varepsilon^2Y_{25}+2\pi nY_{29}),$$
$$Y_{29}'=(H-1)(-2\chi^2(Y_3-Y_{13}-Y_{23})+2\pi n\varepsilon^2Y_{28}),$$
$$Y_{30}'=(H-1)(-2\chi^2(Y_4-Y_{14}-Y_{24})-2\pi n\varepsilon^2Y_{27}),$$
$$Y_{25}'=0,$$
$$Y_{26}'=0,$$

In addition, we have 12 equations that follow from the definitions of the Y_is,

$$hY_5 = -2\pi nY_2h + Y_3',$$
$$hY_6 = 2\pi nY_1h + Y_4',$$
$$Y_7 = (\phi/h + \theta_1/(1-h))Y_1' - 2\pi n\varepsilon^2\phi Y_4 - (\psi/h)Y_2' - 2\pi n\varepsilon^2\psi Y_3$$
$$-\theta_1 Y_{11}'/(1-h) + 2\pi n\varepsilon^2\theta_1(Y_4 - Y_{14}),$$
$$Y_8 = (\phi/h + \theta_1/(1-h))Y_2' + 2\pi n\varepsilon^2\phi Y_3 + (\psi/h)Y_1' - 2\pi n\varepsilon^2\psi Y_4$$
$$-\theta_1 Y_{12}'/(1-h) - 2\pi n\varepsilon^2\theta_1(Y_3 - Y_{13}),$$
$$Y_{15}(1-h) = -2\pi n(Y_2 - Y_{12})(1-h) - (Y_3' - Y_{13}'),$$
$$Y_{16}(1-h) = 2\pi n(Y_1 - Y_{11})(1-h) - (Y_4' - Y_{14}'),$$
$$Y_{17}(1-h) = Y_{11}' - Y_1' - 2\pi n\varepsilon^2(Y_4 - Y_{14})(1-h)$$
$$-\theta_2(Y_1' - Y_{11}' - Y_{21}')(1-h)/(H-1) + 2\pi n\theta_2\varepsilon^2(Y_4 - Y_{14} - Y_{24})(1-h),$$
$$Y_{18}(1-h) = Y_{12}' - Y_2' + 2\pi n\varepsilon^2(Y_3 - Y_{13})(1-h)$$
$$-\theta_2(Y_2' - Y_{12}' - Y_{22}')(1-h)/(H-1) - 2\pi n\theta_2\varepsilon^2(Y_3 - Y_{13} - Y_{23})(1-h),$$
$$Y_{25} = -2\pi n(Y_2 - Y_{12} - Y_{22}) + (Y_3' - Y_{13}' - Y_{23}')/(H-1),$$
$$Y_{26} = 2\pi n(Y_1 - Y_{11} - Y_{21}) + (Y_4' - Y_{14}' - Y_{24}')/(H-1),$$
$$Y_{27} = -2\pi n\varepsilon^2(Y_4 - Y_{14} - Y_{24}) + (Y_1' - Y_{11}' - Y_{21}')/(H-1),$$
$$Y_{28} = 2\pi n\varepsilon^2(Y_3 - Y_{13} - Y_{23}) + (Y_2' - Y_{12}' - Y_{22}')/(H-1).$$

These equations are rearranged into the form $Y_i' = F_i(X, Y_1, \ldots, Y_{30})$ for $i = 1, \ldots, 30$, and then solved numerically.

References

Albers, G.M., Tomkiewicz, R.P., May, M.K., Ramirez, O.E., Rubin, B.K., 1996. Ring distraction technique for measuring surface tension of sputum: Relationship to sputum clearability. J. Appl. Physiol. 81(6), 2690–2695.

Barlow, E., 2000. Modelling muco-ciliary transport in the lung. Master's thesis, School of Mathematics and Statistics, University of Birmingham.

Barton, C., Raynor, S., 1967. Analytical investigation of cilia induced mucous flow. Bull. Math. Biophys. 29, 419–428.

Blake, J.R., 1972. A model for the micro-structure in ciliated organisms. J. Fluid Mech. 55, 1–23.

Blake, J.R., 1973. Mucus flows. Math. Biosci. 17, 301–313.

Blake, J.R., 1975a. Fluid flow in fields of resistance. Bull. Aust. Math. Soc. 13, 129–145.

Blake, J.R., 1975b. On the movement of mucus in the lung. J. Biomech. 8, 179–190.

Blake, J.R., 1977. An active porous medium model for ciliary propulsion. J. Theor. Biol. 64, 697–701.

Blake, J.R., Gaffney, E.A., 2001. Modeling aspects of tracer transport in mucociliary flows. In: Salathe, M. (Ed.), Cilia and Mucus: From Development to Respiratory Defense. Dekker, New York, pp. 291–302.

Blake, J.R., Winet, H., 1980. On the mechanics of muco-ciliary transport. Biorheology 17, 125–134.

Boucher, R.C., 1994. Human airway ion transport. Part 1. Am. J. Respir. Crit. Care Med. 150, 271–281.

Boucher, R.C., 2003. Personal communication.

Boucher, R.C., Knowles, M.R., Yankaskas, J.R., 2000. Cystic fibrosis. In: Murray, J.F., Nadel, J.A. (Eds.), Textbook of Respiratory Medicine. Saunders, Philadelphia, PA, pp. 1291–1323.

Chwang, A.T., Wu, T.Y., 1975. Hydrodynamics of the low-Reynolds number flows. Part 2. The singularity method for Stokes flows. J. Fluid Mech. 67, 787–815.

Davis, S.S., Dippy, J.E., 1969. The rheological properties of sputum. Biorheology 6, 11–21.
Devalia, J.L., Sapsford, R.J., Rusznak, C., Toumbis, M.J., Davies, R.J., 1992. The effects of salmeterol and salbutamol on ciliary beat frequency of cultured human bronchial epithelial cells, in vitro. Pulm. Pharmacol. 5(4), 257–263.
Ekberg-Jansson, A., Larsson, S., Löfdahl, C.-G., 2001. Preventing exacerbation of chronic bronchitis and COPD. BMJ 322, 1259–1261.
Fulford, G.R., Blake, J.R., 1986. Muco-ciliary transport in the lung. J. Theor. Biol. 121, 381–402.
Fung, Y.C., 1993. Biomechanics, 2nd ed. Springer, New York.
Gibbs, B.F., Schmutzler, W., Vollrath, I.B., Brosthardt, P., Braam, U., Wolff, H.H., Zwadlo-Klarwasser, G., 1999. Ambroxol inhibits the release of histamine, leukotrienes and cytokines from human leukocytes and mast cells. Inflamm. Res. 48(2), 86–93.
Gueron, S., Liron, N., 1992. Ciliary motion modeling, and dynamic multicilia interactions. Biophys. J. 63, 1045–1058.
Guggino, W.B., 2001. Cystic fibrosis salt/fluid controversy: In the thick of it. Nat. Med. 7(8), 888–889.
Happel, J., 1959. Viscous flow relative to arrays of cylinders. AIChE J. 5(2), 174–177.
Hasani, A., Toms, N., O'Connor, J., Dilworth, J.P., Agnew, J.E., 2003. Effect of salmeterol xinafoate on lung mucociliary clearance in patients with asthma. Respir. Med. 94(6), 667–671.
International Commission on Radiological Protection and Measurements, 1994. Human respiratory tract model for radiological protection—ICRP Publication 66. Ann. ICRP 24, 1+.
Keller, S.R., 1975. Fluid mechanical investigations of ciliary propulsion. PhD thesis, California Institute of Technology.
Kerem, E., Bistritzer, T., Hanukoglu, A., Hofmann, T., Zhou, Z., Bennett, W., MacLaughlin, E., Barker, P., Nash, M., Quittell, L., Boucher, R., Knowles, M.R., 1999. Pulmonary epithelial sodium-channel dysfunction and excess airway liquid in pseudohypoaldosteronism. N. Engl. J. Med. 341, 156–162.
King, M., Agarwal, M., Shukla, J.B., 1993. A planar model for muco-ciliary transport: Effect of mucus viscoelasticity. Biorheology 30, 49–61.
Liron, N., Mochon, S., 1976. The discrete-cilia approach to propulsion of ciliated micro-organisms. J. Fluid Mech. 75, 593–607.
Liron, N., Rozenson, M., 1983. Muco-ciliary transport. J. Submicrosc. Cytol. 15(1), 317–321.
Lutz, R.J., Litt, M., Charkrin, L.W., 1973. Physical–chemical factors in mucus rheology. In: Gabelnick, H.L., Litt, M. (Eds.), Rheology of biological systems. Charles C. Thomas, Springfield, IL, pp. 119–157.
Matsui, H., Randell, S.H., Peretti, S.W., Davis, C.W., Boucher, R.C., 1998. Coordinated clearance of periciliary liquid and mucus from airway surfaces. J. Clin. Invest. 102(6), 1125–1131.
Meyer, F.A., Silberberg, A., 1980. The rheology and molecular organization of epithelial mucus. Biorheology 17, 163–168.
Pavia, D., Bateman, J.R., Lennard-Jones, A.M., Agnew, J.E., Clarke, S.W., 1986. Effect of selective and non-selective beta blockade on pulmonary function and tracheobronchial mucociliary clearance in healthy subjects. Thorax 41(4), 301–305.
Poole, P.J., Black, P.N., 2001. Oral mucolytic drugs for exacerbations of chronic obstructive pulmonary disease: Systematic review. BMJ 322, 1271–1274.
Puchelle, E., Herard, A.L., Zahm, J.M., 1998. Airway mucociliary epithelium injury and repair. In: Baum, G.L., Priel, Z., Roth, Y., Liron, N., Ostfeld, E.J. (Eds.), Cilia, Mucus, and Mucociliary Interactions. Dekker, New York, pp. 203–217.
Puchelle, E., Zahm, J.M., Quemada, D., 1987. Rheological properties controlling mucociliary frequency and respiratory mucus transport. Biorheology 24, 557–563.
Quemada, D., 1984. Towards a unified model of elasto-thixotropy of biofluids. Biorheology 21, 423–436.
Reid, L., 1973. Properties of mucus. Sci. Basis Med. Annu. Rev. 149, 130–150.
Rochat, T., Lacroix, J.S., Jornot, L., 2004. *N*-Acetylcysteine inhibits Na^+ absorption across human nasal epithelial cells. J. Cell Physiol. 201(1), 106–116.
Rogers, D.F., 2004. Airway mucus hypersecretion in asthma: An undervalued pathology? Curr. Opin. Pharm. 4, 241–250.
Rogers, D.F., 2005. Mucociliary disfunction in COPD: Effect of current pharmacotherapeutic options. Pulm. Pharm. Ther. 18, 1–8.
Ross, S.M., 1971. A wavy wall analytic model of muco-ciliary pumping. PhD thesis, John Hopkins University.

Salathe, M., O'Riordan, T.G., Wanner, A., 1996. Treatment of muco-ciliary disfunction. Chest 110, 1048–1057.
Salathe, M., O'Riordan, T.G., Wanner, A., 1997. Mucociliary clearance. In: Crystal, R.G., West, P.J., Barnes, P.J., Weibel, E.R. (Eds.), The Lung: Scientific Foundations. Lippincott-Raven, Philadelphia, PA, pp. 2295–2308.
Sanderson, M.J., Sleigh, M.A., 1981. Ciliary activity of cultured rabbit tracheal epithelium: Beat pattern and metachrony. J. Cell Sci. 47, 331–341.
Shibuya, Y., Wills, P.J., Cole, P.J., 2003. Effect of osmolality on mucociliary transportability and rheology of cystic fibrosis and bronchiectasis sputum. Respirology 8(2), 181–185.
Silberberg, A., 1983. Biorheological matching: Mucociliary interaction and epithelial clearance. Biorheology 20, 215–222.
Sleigh, M.A., 1977. The nature and action of respiratory tract cilia. In: Brain, J.D., Proctor, D.F., Reid, L.M. (Eds.), Respiratory defense mechanisms Part I. Dekker, New York, pp. 247–288.
Sleigh, M.A., Blake, J.R., Liron, N., 1988. The propulsion of mucus by cilia. Am. Rev. Respir. Dis. 137, 726–741.
Smith, D.J. 2006. Modelling muco-ciliary transport in the lung. PhD thesis, University of Birmingham, UK.
Smith, D.J., Gaffney, E.A., Blake, J.R., 2006. A model of tracer transport in airway surface liquid. Bull. Math. Biol., submitted for publication.
Smith, J.J., Travis, S.M., Greenberg, E.P., Welsh, M.J., 1996. Cystic fibrosis airway epithelia fail to kill bacteria because of abnormal airway surface liquid. Cell 85, 229–236.